Evolutionary tempo and mode of *Triceratops* from the uppermost Maastrichtian Frenchman Formation of southern Saskatchewan.

By

Mathew James Roloson

A thesis submitted to the Faculty of Graduate and Postdoctoral Affairs
in partial fulfilment of the requirements for the degree of

Master of Science

in

Earth Sciences

Carleton University
Ottawa, Ontario

Abstract

Previous work regarding the upper Maastrichtian Hell Creek Formation of Montana has hypothesized that two temporally separated species of *Triceratops* were anagenetically related, with the older *T. horridus* having directly given rise to the younger *T. prorsus*. However, this work was limited in geographic scope, and only briefly considered the many known skulls of *Triceratops* found outside the formation. Several such skulls of varying completeness have been found in the uppermost Maastrichtian Frenchman Formation of southern Saskatchewan over the last century, and provide a crucial test of the anagenesis hypothesis. Given that the Frenchman Formation was deposited contemporaneously with the upper Hell Creek Formation, the anagenesis hypothesis predicts that only *T. prorsus* should occur within the Frenchman Formation.

I tested this hypothesis against two alternatives with reference to the available *Triceratops* skull material from the Frenchman Formation, which had not been systematically studied prior to our investigation. Using qualitative comparisons and linear discriminant analyses, I found that nasal horn cores were generally larger, accompanied by a wide, vertically oriented, nasal process of the premaxilla, traits previously associated with the geologically younger *T. prorsus*. Hierarchal cluster analyses, revealed no distinct groupings of *T. prorsus*, implying a homogenous population. Thus, I concluded that all *Triceratops* material from the Frenchman Formation compare most closely to *T. prorsus*. and therefore find support for the original anagenesis hypothesis.

Additionally, I was able to relocated and provide stratigraphic data for six *Triceratops* specimens from the Frenchman Formation. I found no preference in depositional environment, with specimens equally distributed in both sand and mudstone facies. When relatively dated against each other, I found no fine scale trends in morphology had occurred across the latest Maastrichtian, suggesting that *Triceratops* may have been in evolutionary stasis prior to its extinction at the end of the Cretaceous.

Acknowledgements

I would like to thank Dr. Jordan Mallon and Dr. Hillary Maddin for their supervision, guidance, and patience throughout this project, without which I likely would not have finished, and Dr. Michael Ryan and Dr. Emily Standen for their valuable committee feedback. I would like to thank Dr. Jade Atkins for her supportive suggestions and edits. Thanks to the staff and students of Carleton University, especially to the Carleton University Palaeontology students, for their support and encouragement.

Thanks also to the staff of the Canadian Museum of Nature, T. rex Discovery Center, and the Museum of the Rockies for providing access to their collections. Thanks to Dr. Catherine Forster and Dr. John Scannella for their raw datasets. Thanks to Dr. Emily Bamforth and Dr. Hallie Street for their assistance in the field and for completing the RSM P1163.4 quarry.

Thanks to both the Canadian Museum of Nature and Carleton University for funding this project as well as the Dinosaur Research Institute for funding my travels to the Museum of the Rockies.

Special thanks to my partner Anastasia Morris, whose encouragement kept me from giving up multiple times. Finally, I would like to thank my Mother and Father, T.K, Bif, and Ana for their constant love and support.

Table of Contents

List of Tables

List of illustrations

List of Appendices

Institutional Abbreviations

AMNH, American Museum of Natural History, New York, New York; CM, Carnegie Museum**,** Pittsburgh, Pennsylvania; CMN, Canadian Museum of Nature, Ottawa, Ontario; DMNH, Delaware Museum of Nature and Science, Wilmington, Delaware; EM, Eastend Museum, Eastend, Saskatchewan; FMNH, Field Museum of Natural History, Chicago, Illinois; LACM, Natural History Museum of Los Angeles County, Los Angeles, California; ROM, Royal Ontario Museum, Toronto, Ontario; RSM, Royal Saskatchewan Musuem, Regina, Saskatchewan; SMM, Science Museum of Minnesota, Saint Paul, Minnesota; TMP, Royal Tyrrell Museum of Palaeontology, Drumheller, Alberta; UND, University of North Dakota, Grand Forks, North Dakota; USNM, Smithsonian National Museum of Natural History, Washington, DC; YPM, Yale Peabody Museum**,** New Haven, Connecticut;

Chapter 1: Evolutionary Mode of Canadian *Triceratops*

Introduction

Understanding the diversity of and evolutionary relationships between species has been a primary goal of paleontologists for decades. Although the study of genetics has revolutionized our understanding of many aspects of evolution, it cannot shed light on the long-term records of natural population change occurring over thousands or millions of years. For example, geneticists may be able to record what happens to a population of *Drosophila* over a period of several years under controlled conditions, but those results do not necessarily reflect what would occur to that same lineage under natural conditions, and over the course of a century (Simpson, 1984). While these laboratory studies can reveal microevolutionary trends, it is quite possible that those trends differ both quantitatively and qualitatively when applied to macroevolutionary scales. Paleontology uniquely provides a dimension of deep time not otherwise available and can assist in testing and validating those concepts first proposed in laboratory studies (Allen & Briggs, 1989; Wagner, 2020). Two concepts that benefit from the paleontological perspective are those of evolutionary tempo and mode (Simpson, 1984).

Evolutionary Tempo and Mode

Evolutionary tempo refers to the rate at which evolution occurs. This includes both the speed and acceleration of speciation, and can be broken down into two opposing theories: gradualism, or the slow continuous accumulation of traits resulting in eventual speciation, and punctuated equilibrium, whereby speciation occurs rapidly and is then followed by long periods of evolutionary stasis (Johnson, 2011).

Evolutionary mode describes the manner or pattern of evolution and has historically been dichotomized into two pathways: cladogenesis and anagenesis (Fig. 1.1). However, these terms are inconsistently used and vaguely defined in modern disciplines. A third term, anacladogenesis, has recently been used in many extant island biogeographical studies, but has yet to gain widespread use in paleontological studies (Meiri et al., 2012; Emerson and Patiño, 2018). Because each mode requires different conditions to occur, it is important to clearly define and differentiate between them if inferences about paleoecology or other evolutionary relationships are to be made.

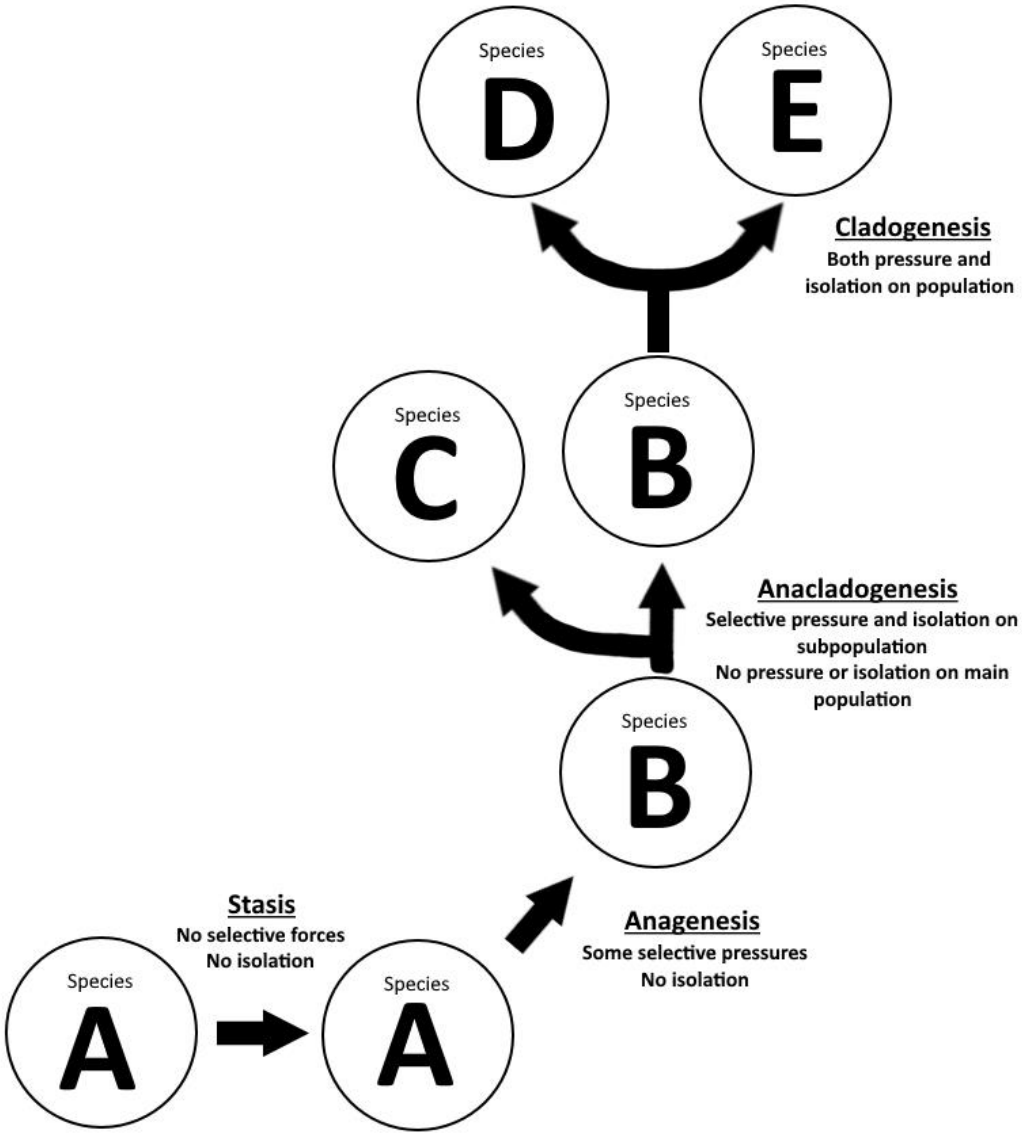

Figure 1.1: Diagram showing various evolutionary modes.

Cladogenesis (from the Greek clados, “branch” and genesis “origin”) describes the branching of evolutionary lineages, whereby a founder population divides into two or more reproductively isolated lineages, typically via allopatric speciation (Gould and Eldredge, 1977; Stanley, 1979; Johnson, 2011; Strotz and Allen, 2013; Emerson and Patiño, 2018). Cladogenesis requires that some form of reproductive isolation occurs and that one or more selective pressures exist on all descendant subpopulations. An example of this can be found in the freshwater Lake Malawi, in which a single, now extinct species of cichlid diverged into more than 850 species over the last 2 million years (Gante and Salzburger, 2012). Because the lake is now a closed body of water, both resource allocation and niche partitioning act as selective forces, and are coupled with intense sexual selection by females, promoting rapid speciation.

Anagenesis (from the Greek ana, “up”, referring to directional change, and genesis, “origin”) contrasts with cladogenesis, and refers to the gradual and direct evolution of a lineage without a splitting event (Futuyma, 1987; Emerson and Patiño, 2018). Anagenesis implies that the founding population changes over time, primarily through mutation and recombination events, resulting in a new species completely replacing the ancestral species (Futuyma, 1987; Vaux, et al, 2016). Anagenesis requires that some selective force on the entire population be present and that no reproductive isolation occurs. As such, it is generally considered a slow process, as small variations must accumulate through the entire population. A recent study using probabilistic phylogenetics found support that anagenesis was common within the hominine lineage, with several direct lineage

relationships existing (Parins-Fukuchi et al., 2019). This analysis reconstructed *Australopithecus anamensis* as directly ancestral to *Australopithecus afarensis, Homo antecessor* as directly ancestral to *Homo heidelbergensis,* and *Australopithecus garhi* as a direct ancestor to the entire *Homo* clade.

Finally, anacladogenesis is a combination of both cladogenesis and anagenesis that allows for both the divergence of an ancestral species into new species, coupled with the continued existence of said ancestral species (Emerson and Patiño, 2018). Anacladogenesis requires reproductive isolation to occur within some group of the population and one or more different selective forces to be applied to said isolated group. This type of evolutionary divergence is commonplace within island environments, wherein an island is colonized by a mainland species, followed by rapid divergence among the newly isolated subpopulation, whereas their original mainland ancestors are maintained in evolutionary stasis.

Conditions Required to Distinguish Modes of Evolution in the Fossil Record

Distinguishing evolutionary mode within the fossil record first requires a sample size large enough to both spatially and temporally represent the entire population over the desired study range. Chronostratigraphic data must also be collected to establish a relative age. Additionally, anagenesis, cladogenesis, and anacladogenesis each require different levels of reproductive isolation and selective forces to occur. Each mode further entails predictable distributions within the fossil record.

Anagenetic evolution requires that the ancestral species be completely replaced by its descendant species. As such, both species would predictably be completely separated temporally. Furthermore, if an uninterrupted stratigraphic profile exists, one could hypothesize that under an anagenetic scenario, specimens with intermediate morphologies would be found that present some mixture of ancestral and descendant characteristics. Anacladogenetic evolution requires that both the ancestral species and one or more descendant species exist contemporaneously; however, the first appearance date (FAD) of the ancestral species would predictably occur sometime before the FAD of the earliest descendant. Cladogenetic evolution requires that a diversification event occurred, implying that the number of descendant species should exceed the number of ancestral species. Unlike anagenesis, where one species is replaced by another, cladogenesis results in two or more new species replacing the ancestral species.

Again, this would predictably mean that both descendant and ancestor species would be temporally separated.

Difficulties Distinguishing Modes of Evolution in the Fossil Record

Detecting evolutionary mode within the fossil record is problematic due to the difficulties associated with incomplete collection and preservation of specimens. Differences in academic interests and sampling efforts can also vary through time. As a result, not all individuals or species that lived in the past are equally likely to be discovered, creating gaps in phylogenetic reconstructions (Lloyd et al., 2012). Distinguishing evolutionary mode becomes further confounded due to the lack of genetic information in the fossil record, and our reliance solely on morphological features. Any missing lineages may result in a misinterpretation of evolutionary mode and makes differentiating between a direct or branching lineage difficult.

The fossil record contains many well-documented examples of gaps that influence our interpretations of evolution. For example, highly detailed fossil records have been recovered, detailing the phylogenies of modern horses (Cantalapiedra et al., 2017; MacFadden, 2005). A variety of sedimentary characteristics indicate that, during the late Neogene, the climate became progressively more arid, resulting in a shift from primarily forested to more open-prairie habitats dominated by grasses. This climatic shift parallels the evolution of

equine teeth as they adapted from processing leaves to grasses, and in the hind limb morphology of horses as they became efficient, long-limbed runners to assist in outdistancing open-prairie predators (Cantalapiedra et al., 2017; MacFadden, 2005). Originally, a lack of fossil material supported a linear transition (i.e., anagenesis), where each species was replaced by successively better adapted descendant species. However, more recent discoveries have resulted in a reinterpretation of the pattern of equine evolution, resulting in a more complex and multi-branched (cladogenetic) phylogenetic history (Cantalapiedra et al., 2017). These results imply that some form of genetic isolation must have occurred, probably multiple times, during the period of environmental shift. Examples like this, where new fossil materials contrast with our previous simple interpretations of evolutionary modes, suggest the phylogenetic scenario that we construct must be constantly revised as new data becomes available (Erwin and Anstey, 1995).

Triceratops **as a Case Study for Detecting Evolutionary Modes in Dinosauria**

Provided a large enough sample size and detailed chronostratigraphic data, it should be possible to test hypotheses of evolutionary mode for a clade within the fossil record. One genus that represents a prime case study is the horned dinosaur *Triceratops* which is a ceratopsian from the latest Cretaceous of North America. Ceratopsia is defined as all species more closely related to *Triceratops*

than to *Pachycephalosaurus* (Scannella et al., 2014) Ceratopsians are morphologically diagnosed in part by the presence of the rostral bone, composing the upper half of the beak at the front of the skull (Forster, 1996a). The clade first appears in the Late Jurassic of Asia (Yinlong) as small, bipedal herbivores (Xu et al., 2006). Successively more derived forms become larger, obligate quadrupeds, and show a progressive elongation of the parietosquamosal portion of the skull, culminating in the long, often highly ornamented, frills of the Late Cretaceous Ceratopsidae. Ceratopsidae is composed of two clades, Centrosaurinae and Chasmosaurinae, (generally having a less ornate frill, a short nasal horncore, and long postorbital hornores (Scannella et al., 2014)). *Triceratops* was one of the last and largest of the Chasmosaurines to evolve and lived until the very end of Cretaceous.

Like most chasmosaurines, an adult-sized *Triceratops* has two long, robust postorbital horncores, a single, smaller nasal horncore, and a solid parietosquamosal frill (unlike most chasmosaurines) (Marsh, 1889; Forster, 1996a). The genus is highly abundant in the Upper Cretaceous deposits of North America and ranged from western Canada to New Mexico (Fig. 1.2). Available material includes excellent representatives of juvenile, subadult, and adult specimens, that together provide data of a nearly complete ontogenetic sequence (Forster, 1996b; Scannella and Fowler, 2014; Scannella, 2015; Wilson and Fowler, 2017). The postorbital horncores vary in taper, stoutness, curvature, and length, and changed direction through ontogeny, generally curving posteriorly while young and transitioning anterolaterally with increased size and putative age

(Scannella et al., 2014). The nasal horn varies from being a modestly tapered blunt boss (often augmented by an epinasal) to a prominent upward and forward-directed projection (Ostrom and Wellnhoffer, 1985; Forster, 1996b). The parietal-squamosal frill is relatively short compared to other chasmosaurines, elongating with age, and generally curls dorsally along its posterior half (Scannella et al., 2014). Thinning on the body of the parietal has been observed in some of the frills of putatively mature specimens, leading to the suggestions that these regions are precursors to the parietal fenestrae of *Torosaurus*, which has been hypothesized to be the older, more mature stage of *Triceratops* (Scannella & Horner, 2010). The frill margins were adorned with dermal epiossifications (epimarginals) that have a triangular profile in juveniles and subadults. During ontogeny, these epiparietals and episquamosals can go through extreme morphological changes. They can fuse to their underlying frill, and while getting larger during growth, their width expands at a greater rate than their height, often resulting in them becoming low, elongate processes that border the margin of the frill. In some large individuals, the epiossifications completely fuse to the frill, becoming indistinguishable from it.

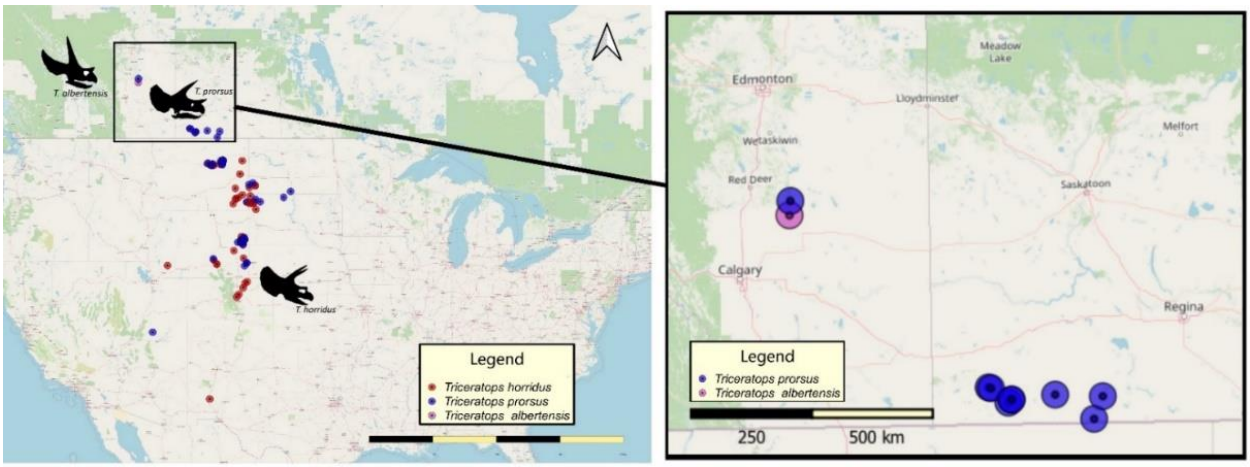

Figure 1.2: Distributions of currently identified *Triceratops* species across entire range. North American range (left), Canadian distribution (right). Maps created using QGIS open-source software (QGIS Development Team, 2020).

The taxonomy of the genus *Triceratops* has been revised several times, and once it included up to 16 species distinguished by small variations in horncore orientation and length, among other subtleties (Ostrom and Wellnhoffer, 1985). By comparing this variation to modern horned analogs, like bovids, Ostrom and Wellnhoffer (1986) proposed that these differences were examples of natural variation within a single species, and reduced the number of species to one, the originally named *Triceratops horridus.* A series of morphometric and cladistic analyses by Forster (1996b) resulted in the separation of the genus into the two currently recognized species: *T. horridus* and *Triceratops prorsus*, distinguished primarily by differences in the nasal horn and snout morphology.

Additional studies on *Triceratops* evolution suggested that these two species formed a direct lineage, with the geologically older *T. horridus* being replaced by the younger *T. prorsus (*Scannella et al,. 2014). These studies used detailed stratigraphic data to relatively date each *Triceratops* specimen within the Hell Creek Formation (HCF) of Montana. *Triceratops horridus* were found to be? limited to the lower third and middle sections of the HCF, whereas *T. prorsus* is restricted to the upper third. The lack of species overlap, combined with several specimens in the middle displaying combinations of both *T. horridus* and *T. prorsus* characteristics, led to the proposal of an anagenetic evolutionary event occurring between the two species (Scannella et al., 2014).

Limitations of Previous Studies

Whereas previous studies have shown support for an anagenetic mode of evolution of *T. horridus* to *T. prorsus*, they did not investigate the entire known geographic range of the genus (Scannella et al., 2014). Instead the HCF (Fig 1.2) represents a relatively small area of the known latitudinal distribution of *Triceratops*. Modern ecological studies have shown that range centres are generally more stable, whereas range limits are characterized as areas of increased genetic isolation, genetic differentiation, and individual variation (Sexton et al., 2009; Nadeau & Urban, 2019). This suggests that the previous study, while representative of localized evolutionary mode, may not represent what is happened to the entire species. Although the evolution of *Triceratops* is well represented within the HCF, the genus also occurs outside the United States, in Alberta within the Scollard Formation (SF) and Saskatchewan within the Frenchman Formation (FF). These locations represent the northern latitudinal range limit of *Triceratops* and thus warrant consideration in order to interpret modes of evolution in this lineage. However, because *Triceratops* is poorly represented within the Scollard Formation, I will focus on material from the Frenchman Formation in this thesis.

Hypotheses and Predictions

The primary goal of this thesis is to re-evaluate the anagenesis hypothesis first proposed by Scannella et al. (2014) within the Hell Creek Formation through the inclusion of material from the Frenchman material, which is contemporaneous with material from the upper 3rd of the HCF. Since both *T. horridus* and *T. prorsus* were found to be separated spatially, with only *T. prorsus* being found with the upper third of the HCF, for anagenesis to be supported, only *T. prorsus* should be present within the contemporaneous FF (Fig 1.3). We should also see no distinction between *T. prorsus* found with the HCF and the FF.

However, at least two alternative hypotheses exist that should also be considered, both cladogenesis and anacladogenesis. If cladogenesis is to be supported, there should be no *T. horridus* found within the FF, similar to anagenesis; however, there must also be a detectable and significant difference between the *T. prorsus* of the HCF and the *T. prorsus* of the FF, such that they might be considered their own species. Alternatively, for anacladogenesis to be supported, we need only find evidence that at least one *T. horridus* was present within the FF.

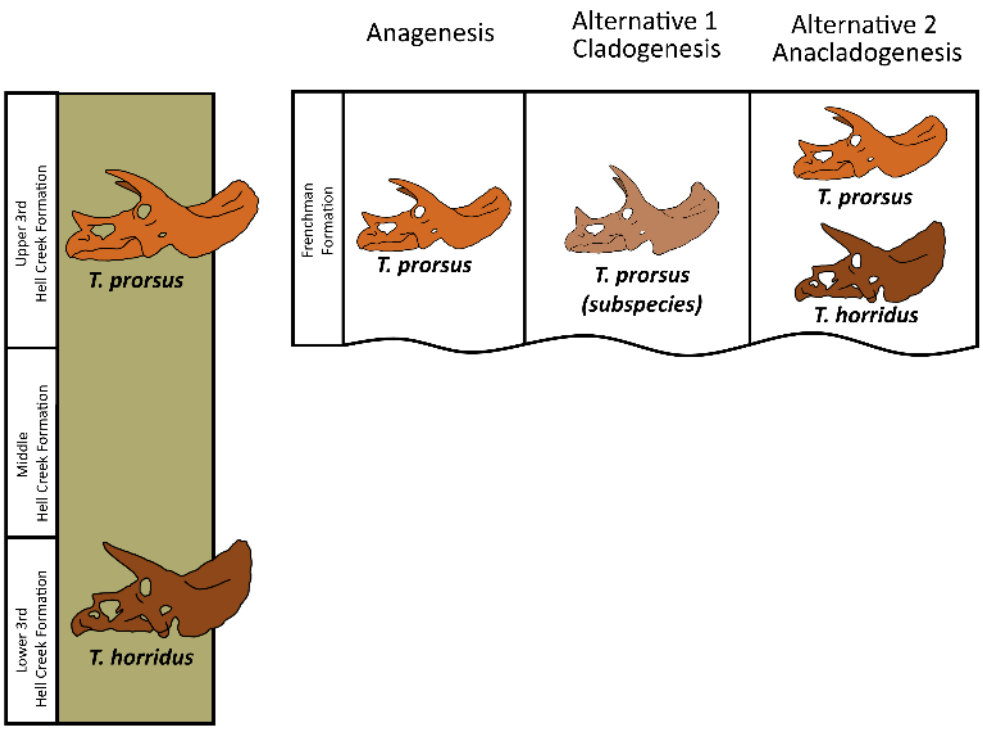

Figure 1.3: Primary hypothesis and alternatives with associated predictions of which species of *Triceratops* to expect within the Frenchman Formation if each alternative was supported.

Thesis Aims and Goals

Triceratops has been found in Canada dating back to as early as 1921 (Sternberg, 1924), and despite nearly a century of discovery, the Canadian *Triceratop*s material remains largely undescribed. Therefore, a primary goal of this project will be to describe the most diagnostic Canadian *Triceratops* specimens. Chapter 2 will include both descriptions and illustrations of seven of the best-preserved *Triceratops* skulls found in Canada, as well as several fragmentary specimens featuring diagnostic characteristics. Using linear measurements of both Canadian and American specimens, I will attempt to quantifiably predict, through canonical variate analysis, whether each Canadian specimen groups with *T. horridus* or *T. prorsus*. Subsequently, the alternative hypotheses of cladogenesis and anacladogenesis will be tested through cluster analysis, and inferences will be made regarding any differences that might exist between the *T. prorsus* of the HCF and any found within the FF.

Additionally, as was typical of early paleontology, limited stratigraphic or geographic information was recorded for many of the Canadian specimens, making it impossible to determine stratigraphic positions of the fossils relative to one another. As such, Chapter 3 will focus on creating a stratigraphic profile of all known Canadian *Triceratops* quarries by relocating the original quarries, and attempting to place them within stratigraphic context of one another using a datum (the K-Pg boundary). This information will then be used to determine the existence of fine-scale morphological trends in *Triceratops*, leading up the

extinction of the non-avian dinosaurs. Chapter 4, the final chapter, will then discuss the overall conclusions, and provide future applications of the findings.

Chapter 2: Classification of *Triceratops* from the Frenchman Formation and implications for evolutionary mode in the fossil record

Introduction

Triceratops horridus and *Triceratops prorsus* are separated stratigraphically within the Hell Creek Formation (HCF) of Montana (Scannella et al., 2014). *Triceratops horridus* is found within the lower third, and lower parts of the middle section of the HCF while *T. prorsus* is restricted to the upper third (Scannella et al., 2014). The stratigraphic segregation of the two species suggests that *T. horridus* and *T. prorsus* do not represent sexual or ontogenetic variation within a single taxon (Scannella et al., 2014). The additional existence of specimens exhibiting a transitional morphology within the middle section of the HCF has led to the hypothesis that anagenesis occurred within *Triceratops*. If this is true, then all material from the Frenchman Formation (FF) of southern Saskatchewan, which is contemporaneous with the upper third of the HCF (Fowler, 2017; Eberth & Kamo, 2019), should be referable to *T. prorsus.* Alternatively, if specimens within the FF are classified as both *T. horridus* and *T. prorsus* then anagenesis must be rejected in favour of anacladogenesis.

While the first recorded specimens of *Triceratops* from the FF were discovered in 1921 (Sternberg, 1924), the first significant summary of the material was published in 1967, mentioning 14 *Triceratops* specimens and one "undetermined long-squamosalled ceratopsian", now classified as *Torosaurus*

(Russell, 1967, 4). Tokaryk (1986) then published a detailed history and partial description of two specimens (RSMH P1163.4 and EM P15.1), identifying both as *T. prorsus*. These descriptions were cursory, and only made note of qualitative potentially diagnostic characters, such as horn size/orientation and rostral shape. Additionally, these specimens were not included in Forsters' (1996b) morphometric analysis which restructured the genus, reducing the number of species of *Triceratops* from 13 to two. Therefore, as these previous attempts to classify the *Triceratops* of the FF were not exhaustive, a revisit is warranted.

Whether the anagenetic trend hypothesized for *Triceratops* in the HCF holds true for the FF depends on an accurate classification of the material. Therefore, the first aim of this chapter is to describe and illustrate all the diagnostic FF material, comparing each specimen to the holotypes of *T. prorsus* and *T. horridus.* Descriptions of specimens will focus largely on diagnostic characters. Since the anagenesis hypothesis requires that the FF material all classify as *T. prorsus*, a linear discriminant analysis (LDA) using previously defined specimens of *T. prorsus* and *T. horridus* will be used to group the unclassified FF material. Within the LDA, if any specimens within the FF unambiguously belong to *T. horridus*, then we must instead support the alternative hypothesis of anacladogenesis, as both ancestral and descendent species would have existed contemporaneously.

Because *T. prorsus* is present across a wide latitudinal range, it is also important to investigate that no morphotypes exist between populations. If there is any indication that a distinguishable difference exists between the *Triceratops* of

the FF and those from the upper third of the HCF, the alternative cladogenesis hypothesis could then be supported. As such, a cluster analysis will be run to determine if any intraspecific groupings of *T. prorsus* can be detected.

Materials and Methods

Specimens Examined

The first step in classifying the FF *Triceratops* specimens will be to provide a brief description of the material present, focusing on characters that have previously been used to distinguish between *T. horridus* and *T. prorsus* (Forster, 1996b; Scannella et al,. 2014). These include nasal and postorbital characters, as well as some that account for frill and face shape (Fig. 2.1). Additionally, any traits that are known to change through ontogeny will be mentioned because mature specimens typically have more pronounced derived characters than juveniles.

Both the holotypes of *T. prorsus* (YPM 1822) and *T. horridus* (YPM 1820) have been extensively described in past publications (Marsh, 1889; Marsh, 1890; Tokaryk, 1986; Dodson, 1996; Forster, 1996a). *Triceratops prorsus* is typified as having laterally narrow postorbital horncores, an elongated frill with broadly convex squamosals, a long, forward projecting nasal horn supported by a wide and vertically oriented nasal process of the premaxilla, and a rostrum that is relatively deep and short with a convexly rounded rostral margin (Forster, 1996b; Scannella et al., 2014).

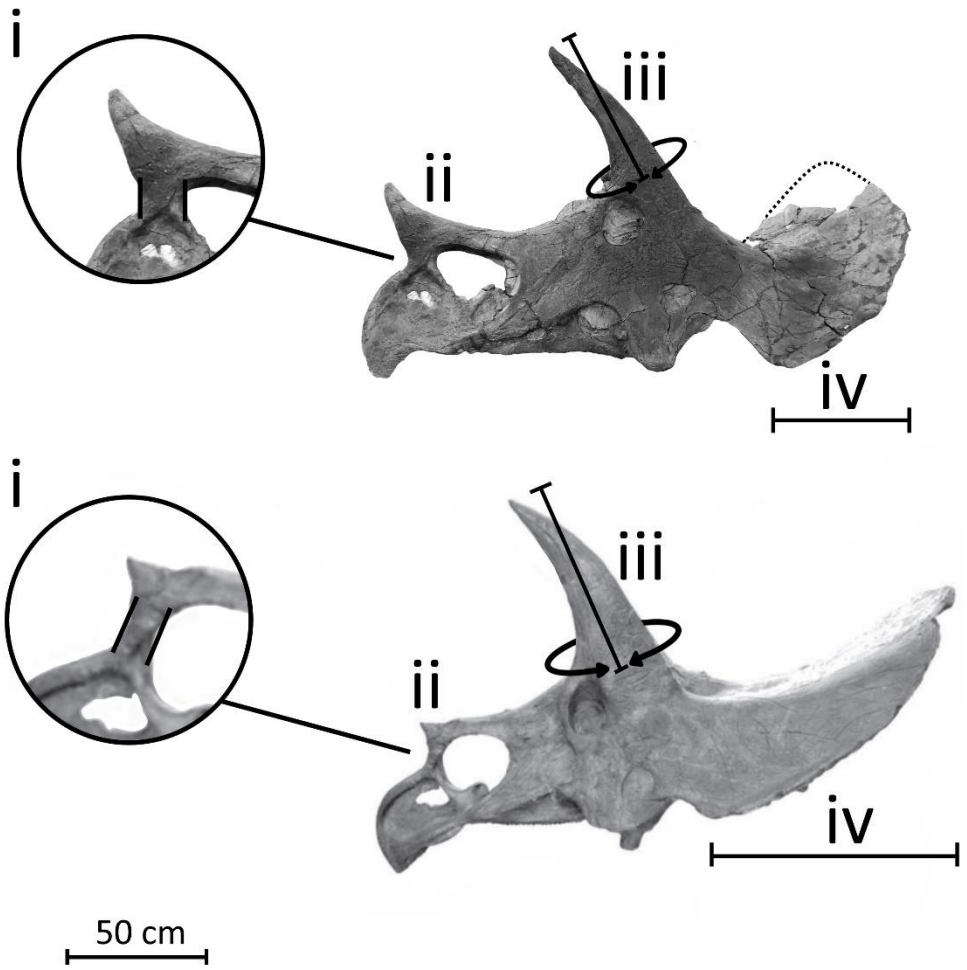

Figure 2.1: Key morphological differences in two species of *Triceratops*, *T. horridus* (bottom, based on SDSM 2760) and *T. prorsus* (top, based on MOR 1604). (i) illustrates variation in width and orientation of nasal process of the premaxilla (NPP) with *T. horridus* having a thinner, posteriorly oriented NPP, and *T. prorsus* having a more robust and vertically oriented NPP; (ii) shows variation in size and shape of nasal horncore length with *T. horridus* having a smaller nasal horncore and *T. prorsus* having a larger nasal horncore; (iii) illustrates variation in length of postorbital horncores with *T. horridus* having larger postorbital horncores which appear circular in cross-section while *T. prorsus* had comparably smaller postorbital horncores that were narrow and occasionally presented with a ventral keel; (iv) displays variation in length and shape of frill with *T. horridus* typically having a more elongate frill while *T. prorsus* had shorter frills with broadly convex squamosals.

Triceratops horridus is characterized as having massive circular postorbital horncores which are longer than those seen in *T. prorsus*. Additionally, *T. horridus* typically have longer frills, and short, blunt nasal horncores, supported by a thinner and posteriorly angled nasal process of the premaxilla.

Scannella et al., (2014) also suggested the presence of an intermediate morpho-species located within the middle of the Hell Creek Formation having a mixture of traits with a convex rostrum morphology associated with *T. prorsus* while retaining the smaller nasal horn cores associated with *T. horridus.* Specimens examined for the present study are listed in Table 2.1.

Table 2.1: List of all *Triceratops* material included in this study.

Specimen ID	Identified Species	Formation	Locality	Material present	Measurement Source
CMN 34824	Unidentified	Frenchman	Saskatchewan	Frill and dorsal skull	Self collected
CMN 8741	Unidentified	Frenchman	Saskatchewan	Frill, and articulated dorsal skull with fragmentary postorbital horncores	Self collected
CMN 56508	Unidentified	Frenchman	Saskatchewan	Frill and articulated postorbital horncores	Self collected
RSM P2982.1	Unidentified	Frenchman	Saskatchewan	Fragmentary skull	Self collected
RSM P1163.4	Unidentified	Frenchman	Saskatchewan	Nearly complete articulated skull	Self collected
EM P15.1	Unidentified	Frenchman	Saskatchewan	Skull, lacking frill and lower face	Self collected
CM 1221	*T. prorsus*	Hell Creek	Montana	Skull	Forster, 1996b
LACM 7207	*T. prorsus*	Hell Creek	Montana	Fragmentary skull	Forster, 1996b
MOR 004	*T. prorsus*	Hell Creek	Montana	Articulated skull	Self collected
MOR 1604	*T. prorsus*	Hell Creek	Montana	Articulated skull	Self collected
MOR 2923	*T. prorsus*	Hell Creek	Montana	Articulated skull	Self collected
MOR 2978	*T. prorsus*	Hell Creek	Montana	Articulated skull	Self collected
SMM P62/1/1	*T. prorsus*	Hell Creek	Montana	Partial skull	Forster, 1996
YPM 1822	*T. prorsus*	Lance	Wyoming	Skull and jaws	Forster, 1996
YPM 1823	*T. prorsus*	Lance	Wyoming	Skull and jaws, lacking nasal and postorbital horncores	Forster, 1996
UND 3000	*T. prorsus*	Hell Creek	Montana	Fragmentary skull	Holland, 1997
AMNH 5116	*T. horridus*	Hell Creek	Montana	Skull	Forster, 1996b
FMNH P12003	*T. horridus*	Hell Creek	Montana	Skull	Forster, 1996b
MOR 1120	*T. horridus*	Hell Creek	Montana	Disarticulated subadult skull (reassembled)	Self collected
USNM 1201	*T. horridus*	Lance	Wyoming	Skull missing nasal horncore, left squamosal is perforated	Forster, 1996b
USNM 2100	*T. horridus*	Lance	Wyoming	Skull lacking rostrum	Forster, 1996b
USNM 2412	*T. horridus*		Wyoming		Forster, 1996b
USNM 4928 / MNHN 1912.20	*T. horridus*	Lance	Wyoming	Skull lacking some parts of the frill, lower jaws	Forster, 1996b
YPM 1821	*T. horridus*	Lance	Wyoming	Skull and dentary	Forster, 1996b
DMNH 48617	*T. horridus*	Denver	Colorado	Skull	Scannella et al., 2014
USNM 4720	*T. horridus*	Lance	Wyoming	Skull	Scannella et al., 2014

Linear Discriminant Analysis

Previous studies have used multivariate principal component analyses (PCA) to differentiate *T. horridus* and *T. prorsus* through cranial features including the length of both nasal and postorbital horns and the shape of the rostrum (Forster 1996b). However, although PCA is useful for determining if groups exist, it cannot be used to quantifiably classify unknown specimens. Instead, using a priori species groupings, unclassified specimens from the FF can be assigned to one of the two groups through use of a linear discriminant analysis (LDA). Unlike PCA, which attempts to maximize variance within a dataset along subsequent PC axes, LDA attempts to maximize the distance between two or more assigned groups, while simultaneously minimizing the within-group variance. Running a LDA on PCA scores that account for a large proportion of the variation, rather than the raw dataset, increases the reliability of the output by reducing the number of input variables for the LDA (Barker & Rayens, 2003).

To complete the LDA, 26 skulls of *Triceratops* were first subjected to PCA using varying subsets of 31 linear skull measurements (Fig 2.2). Ten *T. prorsus*, and ten *T. horridus* specimens from various American upper Maastrichtian formations, and six unidentified *Triceratops* from the Frenchman Formation, were used (Table 2.1). Landmarks, based on previous *Triceratops* morphometric studies, were selected to represent the overall shape and size of the skull, and linear measurements were taken between each landmark (Forster, 1996b; Table 2.2). Measurements < 20 cm were measured to the nearest millimeter using digital calipers, and any measurements >20 cm were measured to

the nearest 0.5 cm using a tailor's tape. Whenever possible, bilateral measurements were taken and averaged; however, because distortion is common in *Triceratops* skulls, the measurements of any heavily distorted skulls were excluded. Three subsets of data were created due to an incomplete dataset. The first analysis contained all variables that were > 50% complete, the second included only those variables present in most of the Canadian skulls (> 50% complete), so as to emphasize those measurements that best characterize them, and the third used only variables that represented diagnostic characters identified in previous studies (Forster, 1996b; Scannella et al., 2014; Table 2.2). Since PCA requires a complete dataset, any missing variables for *T. horridus* and *T. prorsus* were imputed individually for each species and data subset using a Bayesian Principal Component Analysis on the log-transformed data in the R programming suite and base packages, as well as the 'pcaMethods' package (Stacklies et al., 2007; Brown et al., 2012; Community, 2018). Missing variables for the FF material were then similarly imputed using the combined imputed datasets for *T. prorsus* and *T. horridus*.

Z-scores were taken to centralize the data, and all three subsets of the imputed datasets were subjected to PCA using a variance-covariance matrix in PAST V4.03 (Hammer et al., 2001). Each set of PCA scores obtained were then submitted to LDA in PAST.

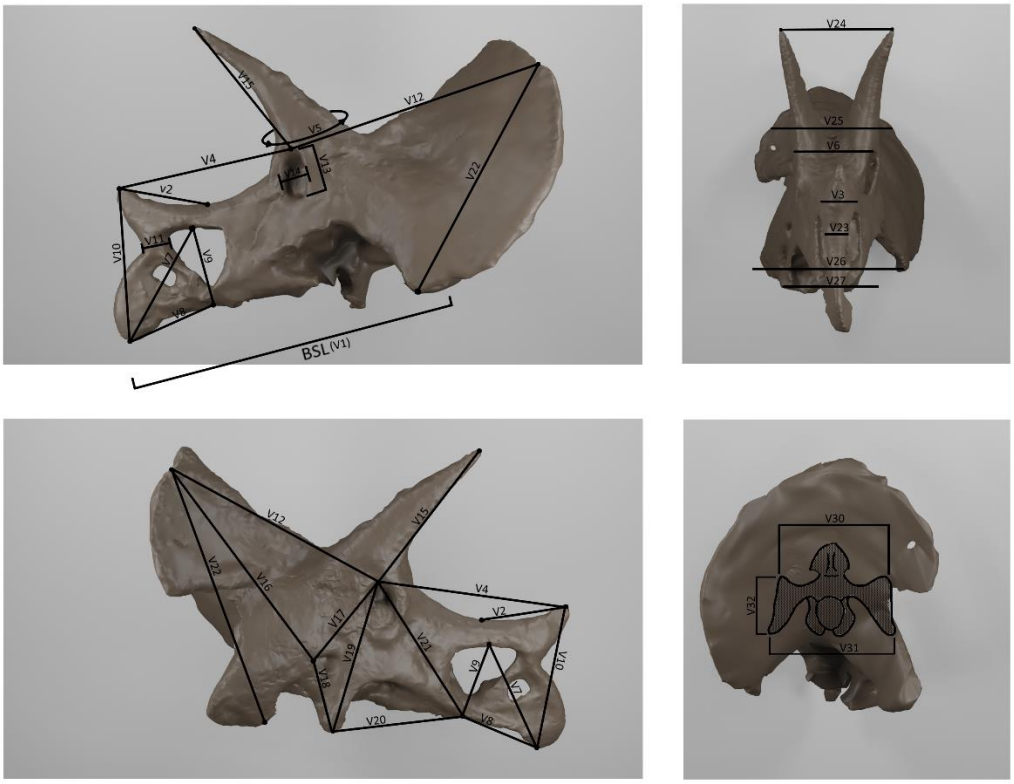

Figure 2.2: 3D render of RSM P1163.4 showing all linear measurements taken on the specimen sample. Model rendered in Blender V2.9 using Meshroom 2021.1.0 (Carsten et al., 2021)

Table 2.2 List of variables included in each data subset as illustrated in Fig 2.2. Variables are discontinuous since not all variables initially collected were complete enough to include in analyses.

Variables	Analysis 1 All variables which are present in at least 50% of the dataset	Analysis 2 All variables which are present in at least 50% of the Canadian material	Analysis 3 All variables considered diagnostic characters
2 - Nasal horncore length measured from tip of nasal horn to nasal-premaxilla contact	included	included	included
3 - width of nasal, measured transversely across nasals at nasal premaxilla contact	included	included	included
4 - linear measurement from the tip of nasal horn to dorsal most rim of orbit	included	included	included
5 - circumference of the postorbital horn base	included	included	included
6 - transverse width from dorsal most rim of orbit to dorsal most rim of orbit	included		
7 - linear measurement from tip of rostral to nasal-premaxilla contact beneath nasal horn	included	included	included
8 - linear measurement from tip of rostral to premaxilla-maxilla contact at tooth row	included	included	included
9 - linear measurement from nasal-premaxilla contact beneath nasal horn to premaxilla-maxilla contact at tooth row	included	included	included
10 - linear measurement from tip of rostral to tip of nasal horn			included
11 - maximum lateral length of nasal process of the premaxilla		included	included
12 - linear measurement from dorsal most rim of orbit to parietal-squamosal contact at caudal frill margin		included	
13 - Maximum Height of orbits		included	
14 - Maximum Width of orbits	included	included	
15 - linear measurement from tip of post orbital horncore to dorsal most rim of orbit		included	included
16 - linear measurement from the squamosal-quadratojugal contact at lower temporal fenestra to parietal-squamosal contact at caudal frill margin	included	included	
17 - linear measurement from postorbital-jugal contact at orbit to squamosal-quadratojugal contact at lower temporal fenestra	included	included	
18 - linear measurement from squamosal-quadratojugal contact at lower temporal fenestra to ventral tip of jugal	included		
21 - linear measurement from premaxilla-maxilla contact at tooth row to dorsal most rim of orbit	included		
22 - linear measurement from parietal-squamosal contact at caudal frill margin to ventral most edge of squamosal		included	
27 - width of skull measured transversely from ventral tip of jugal to ventral tip of jugal	included		
28 - Width of occipital condyle	included		
29 - Height of occipital condyle	included		

Cluster Analysis

In addition to the previous anagenesis hypothesis, multiple alternative hypotheses exist. To determine if support exists for the alternative cladogenesis hypothesis, we must consider and test whether populations of *T. prorsus* from the Frenchman Formation and those found further south are significantly different from on another. This can be tested through a cluster analysis, which clusters specimens that exhibit similar features, while simultaneously differentiating clusters that are dissimilar to each other. These clusters allow for the segmentation of specimens into any number of distinct groups. Because the number of possible *T. prorsus* groups will be identified from the data itself, as opposed to having a known number of groups needed for a K-means cluster analysis, a hierarchical cluster analysis will be used.

Hierarchical clustering algorithms work by iteratively connecting each specimen with the specimen that shares the most number of similar characters with. In contrast to LDA, where each unknown individual is assigned to a known group, a cluster analysis seeks to discover the number and composition of any groups that may be present. Initially each specimen is treated as its own cluster. Next, the two closest specimens are connected, forming a secondary cluster. Then, the two next closest specimen groups (or clusters) are connected to form a larger cluster. The process is repeated until all specimens are connected into a single cluster (Valentine and Peddicord, 1967; Bennington and Bambach, 1996). Finally, the dendrogram that is produced can be interpreted through applying cut-off thresholds at various distances until the desired number of groups are

obtained. While there are various statistical approaches to determine the optimal number of groups, for this study the cut off threshold will be set at the level that best differentiates *T. prorsus* from *T. horridus,* as those two groups are known to be distinct a priori.

Three hierarchical cluster analyses using the PCA scores from the previous LDA data subsets were created. An unweighted pair group method with arithmetic mean (UPGMA) cluster algorithm was chosen in Past version 4.01 (Hammer et al., 2001), using a Euclidean similarity index (chosen because the linear measurements are continuous). All cluster analyses were unconstrained to determine if any natural grouping was occurring.

Results

Specimen Descriptions

CMN 8598

CMN 8598 (Fig 2.3) is an isolated nasal horncore and tip of premaxilla, discovered in 1921 by Charles M Sternberg near Rocky Creek, just outside Wood Mountain within the eastern block of what is now Grasslands National Park, Saskatchewan (Sternberg, 1924). The nasal horncore is approximately 324 mm long measured laterally from the tip to the nasal premaxilla contact, with a maximum basal circumference of 612 mm. The size of the nasal horncore indicates that this individual was likely mature, comparable in size to the larger FF specimens. The dorsal side of the nasal horncore is broad and flat; however, a slight ridge forms at the midline of the posterior end (Fig. 2.3). The horncore is elongate, projects anteriorly and curls posteriorly along its length, like the holotype of *T. prorsus* (YPM 1822). The horncore presents with a slight deformational bend towards the right, with the left tip showing some erosional damage (Fig. 2.3). The ventral side of the horncore is well preserved, with the paired tips of the premaxilla diverging posteriorly, creating a “W” shaped suture

Figure 2.3: Nasal horncore of CMN 8598 in dorsal (a), right lateral (b) and anterior (c). The horncore projects anteriorly and curls posteriorly along its length (b) and displays characteristic "W" shaped suture line (c) both of which are *T. prorsus* traits.

CMN 8741

CMN 8741 (Fig 2.4) was excavated in 1929 by Charles M. Sternberg from the southern end of the East block of Grasslands National Park. It consists of the right frill, posterior portions of the right face, as well as several fragmentary left dentary and postorbital horns (Fig. 2.4). The face is broken along both the prefrontal-lacrimal boundary and the jugal-maxilla boundary, and all material anterior of said break is missing. Extrapolating overall size using the preserved dentary, gives an estimated basal skull length of 120 cm long, which is indicative of its mature status (Horner and Goodwin, 2006). Both postorbital horncores and the frontal bones are disarticulated or missing. The fragmentary pieces of horncore that are present curve anteriorly and are oval in cross section, a trait usually associated with *T. prorsus*; however, because the base of the horncores are missing, life orientation is difficult to determine. CMN 8741 also includes a right quadrate and occipital condyle, but much of this material is reconstructed and was therefore not measured. The frill is rugose and sulcate, indicative of a mature specimen (Horner and Goodwin, 2006). There is mild thinning on the parietal near the squamosal-parietal boundary, but no fenestrae are present (Fig. 2.4). The ventral margin of the right squamosal extends anteriorly, in the form of a slight hook. There are six left episquamosals, which have anteriorly facing apices and are flattened and fused to the external margin of the squamosal, indicating a mature age (Horner et al., 2008). Only four epiparietals are still preserved and are compressed dorsoventrally with the wide ventral surfaces. Without the front of the

face and the nasal horncore, species level identification is difficult based on qualitative descriptions alone. However, the small size and narrow shape of the fragmented postorbital horncore, suggest that the specimen's identification as a *T. prorsus* is more likely.

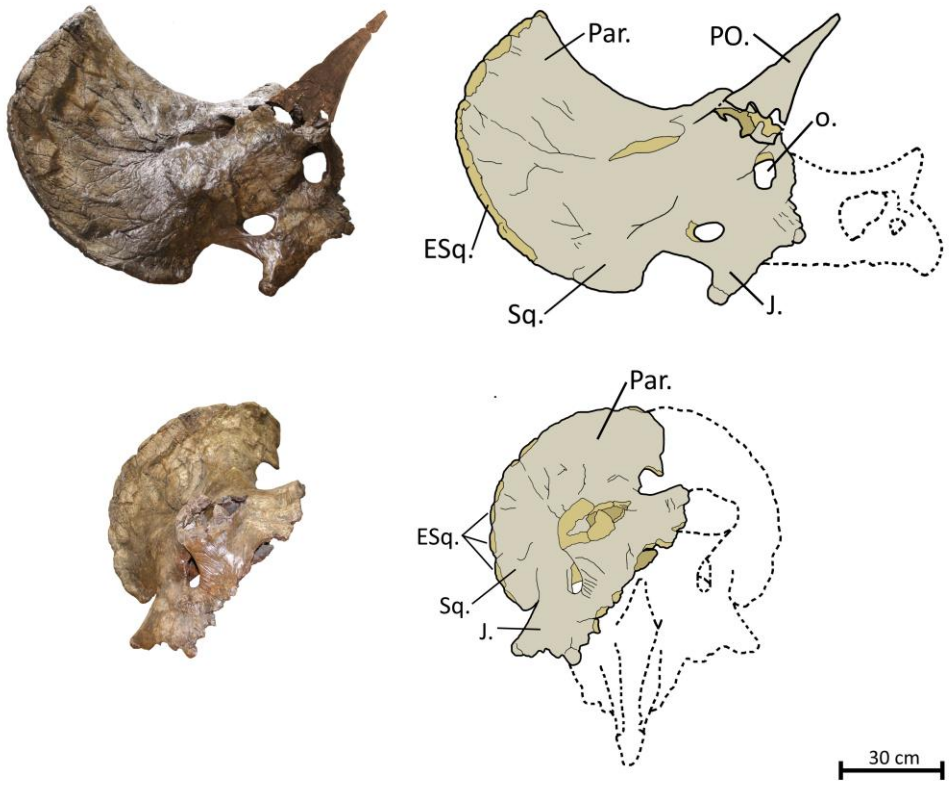

Figure 2.4: Skull of CMN 8741 in lateral (above) and anterior (below) views. Photographs (left) and line drawings (right) with labeled features. Abbreviations: ESq., episquamosals, J., jugal, O., orbit, Par., parietal, PO., postorbital horncore, Sq., squamosal.

CMN 56508

CMN 56508 was discovered by Charles M. Sternberg in 1929, ~10 km west of Eastend, Saskatchewan. A majority of the frill and the top of the skull were preserved with both postorbital horncores (Fig. 2.5). The skull is broken along the jugal-postorbital suture, with the lower half missing. All material anterior to the postorbital is missing, although the dorsal margin of the lacrimal is present. Extrapolating total size by comparing to the nearly complete RSM P1163.4 skull results in an estimated basal skull length of 145 cm, making it the largest specimen in this study. The postorbital horncores are massive and oval in cross-section but taper to a blunt edge on the dorsal side, a trait commonly found in *T. prorsus*. The horncores are uniquely short and taper to a chiseled distal edge. The horncores measure approximately 35 cm along their dorsal margin from the tip to base. Normally, shorter horncores are diagnostic of *T. prorsus*; however, CMN 56508's horncores are relatively shorter than the holotype *T. prorsus*. While there is some erosional damage to the tip of the left horncore, the right horncore appears smooth and unbroken, indicating a natural terminus. The surface of the frill is largely fragmentary, making surface texture difficult to determine. The right parietal overlays the posterior end of the squamosal, indicative of taphonomic distortion. The left parietal is disarticulated and displays extensive thinning, with some medial portions measuring less than 1 cm thick; however, no fenestrae are present. The epi-ossifications, which are also fragmentary, are flat and fused to the frill, which is indicative of a mature individual.

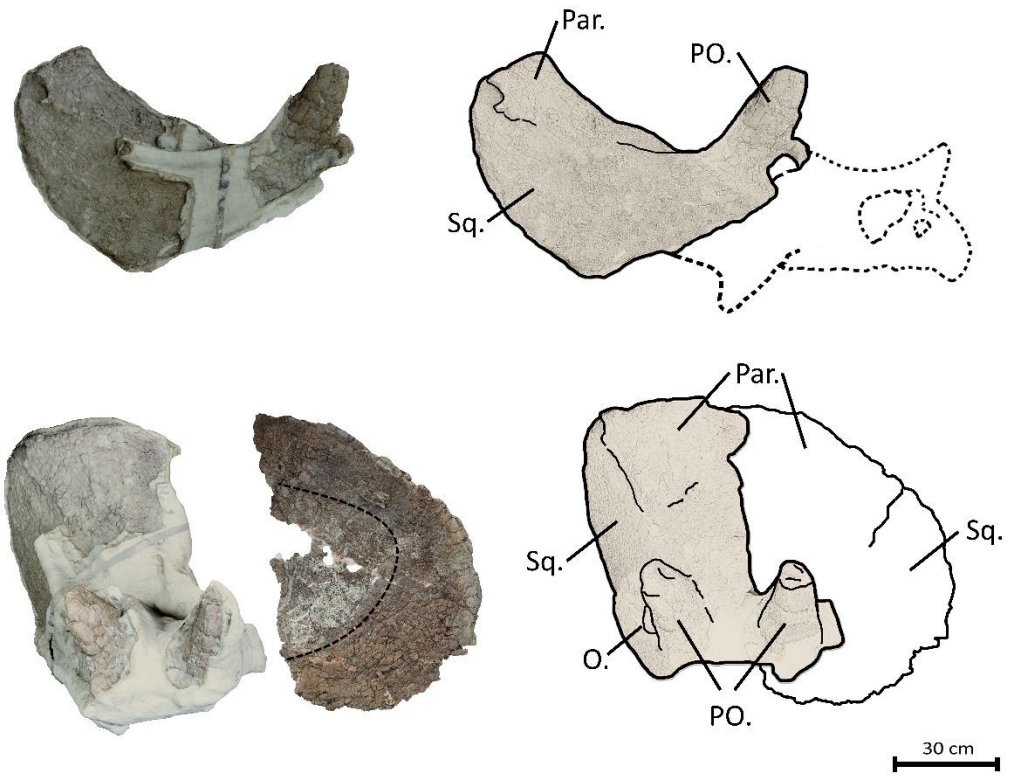

Figure 2.5 Skull of CMN 56508 in lateral (above) and anterior (below) views. 3D renders (left) and line drawings (right) with labeled features. The left parietal shows partial thinning (presented with dotted line). Abbreviations: O., orbit, Par., parietal, PO., postorbital horncores, Sq., squamosal.

EM P15.1

Discovered by Harold Saunders "Corky" Jones, Charlie Holmes, and George Beane in 1936, EM P15.1 was found south of Eastend, Saskatchewan, along the south side of the Frenchman River. It is a largely fragmentary skull, which includes large portions of the upper face and horncores, but is missing the frill, maxilla, and jugals (Fig. 2.6). The suture between the rostral and maxilla is well defined in EM P15.1 indicating that it was subadult (Horner & Goodwin, 2006). The nasal horncore is large and blunt and curves posteriorly, similar to that seen in the holotype of *T. prorsus*, and there is a small shelf on the dorsal edge where the horn meets the remainder of the nasal. Poor preservation prevents an accurate assessment of suture fusion, but the individual was most likely a small subadult with a basal skull length of approximately 85 cm long. The nasal process of the premaxilla is wide, creating a less acute angle between the nasal horn and rostrum than those typical of *T. horridus* and more characteristic of *T. prorsus* (Scannella et al., 2014). The dorsal surfaces of the postorbital horncores are flat and broad, and both curve anterolaterally, with some distortion seen in the tip of the left horncore.

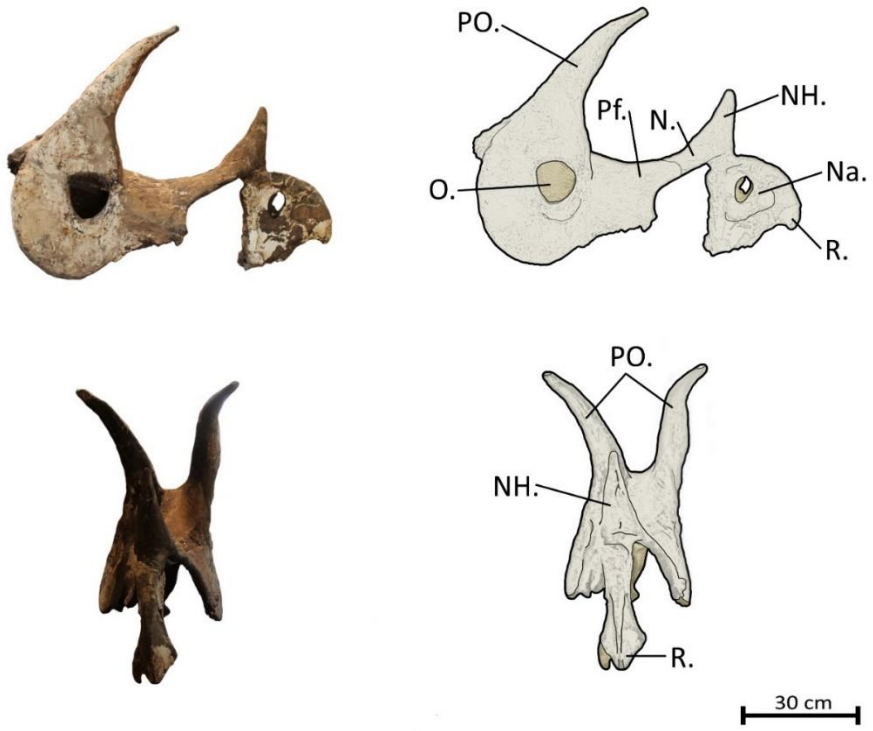

Figure 2.6: Skull of EM P15.1 in lateral (above) and anterior (below) views. Photographs (left) and line drawings (right) with labeled features. Abbreviations: N., nasal, Na., nares, NH., nasal horncore, O., orbit, Par., parietal, Pf., prefrontal bone, PO., postorbital horncores, R., rostrum.

CMN 8864

CMN 8864, an isolated nasal horncore, was discovered in 1946 by Charles M. Sternberg within the Frenchman Formation of southern Saskatchewan. The exact co-ordinates are unknown, but Sternberg's field notes describe the location as being "1.5 miles N.E. of the Frenchman River", roughly 20 km south of Shaunavon, Saskatchewan (C.M. Sternberg, 1946). Sternberg also noted that an isolated dentary was found 25 feet (approximately 7.5 m) from the nasal; however, its whereabouts is currently unknown. The nasal horncore is approximately 413 mm long measured laterally from the tip to the lateral margin of the nasal-premaxilla contact, the end of which is mildly eroded, to the anterior margin of the base (Fig 2.7). The nasal horncore curves posteriorly, a characteristic seen in both subadult and mature *T. prorsus* (Horner & Goodwin, 2006; Scannella et al., 2014). The widest circumference of the nasal horn measures approximately 508 mm. The ventral side of the nasal is eroded such that no sutures are visible however, it still maintains a wide attachment area for the nasal process of the premaxilla, characteristic of *T. prorsus* (Scannella et al., 2014)

Figure 2.7: Nasal horncore of CMN 8864 in right lateral (left) and dorsal (right) views.

CMN 34824

CMN 34824 was collected by Wann Langston, Jr. in 1962 within the Frenchman Formation in what is now the East Block of Grasslands National Park (Langston, 1962). It includes a majority of the frill and the right side of the skull (Fig. 2.8), in addition to a majority of the appendicular skeleton (data not shown). The prefrontals are broken just below the postorbital horncores, preserving the dorsal-most section of the orbit (both the lacrimal and anterior part of jugal are missing). Both postorbital horncores are broken near the base; however, a maximum circumference of 484 mm was obtained from the base of the right horncore. Field notes and photos indicate that the postorbital horncores were present during collection (Langston, 1962); however, their current whereabouts are unknown. The frontoparietal fontanelle is closed, which is typically indicative of a more mature individual (Forster, 1996a); however, the estimated basal skull length is only approximately 75 cm, smaller than most of the other specimens in this study. Scannella et al. (2014) also noticed that the frontoparietal fontanelle closes at an earlier ontogenetic stage in *T. prorsus* than *T. horridus.* The episquamosals are incompletely fused, suggesting that CMN 34824 was more likely a subadult. There are six episquamosals preserved on the right squamosal, and two are present on what remains of the left. The episquamosals are triangular and curve anteriorly. Four epiparietals are distinguishable along the margin of the parietal, all of which are triangular and incompletely fused, indicating the individual was not mature. The frill surface is poorly preserved and either

fragmentary or smooth with little detail. The left side of the frill displays some taphonomic distortion and is pushed anteriorly.

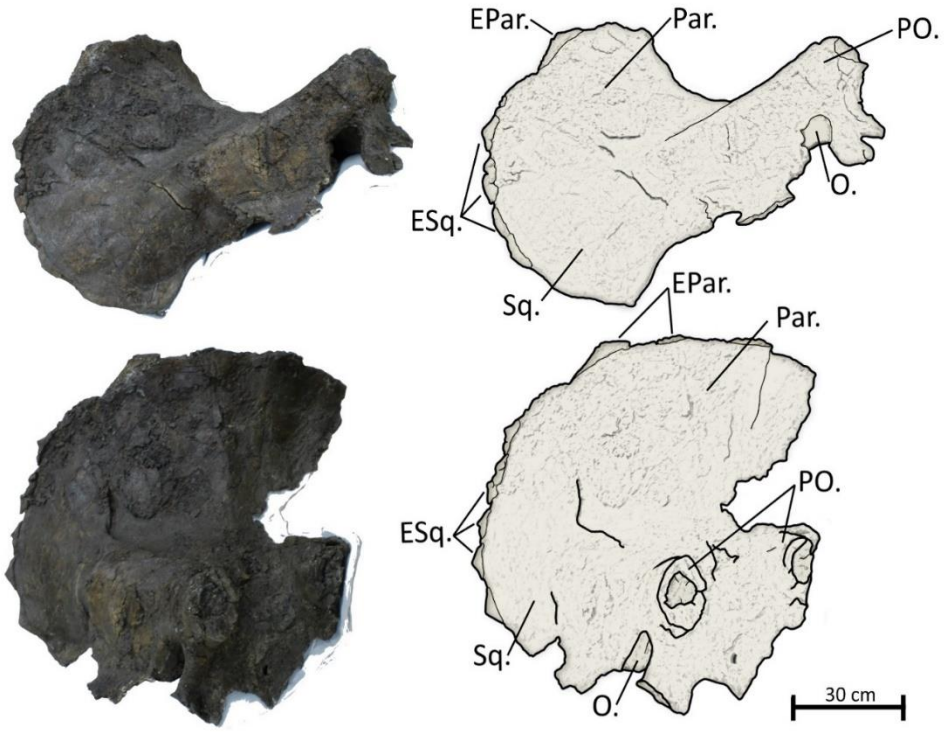

Figure 2.8: Skull of CMN 34824 in lateral (above) and anterior (below) views. Photographs (left) and line drawings (right) with labeled features. Abbreviations: EPar., epiparietal, ESq., episquamosals, O., orbit, Par., parietal, PO., postorbital horncores, Sq., squamosal.

RSM P1163.4

RSM P1163.4 is a nearly complete skull found by the Royal Saskatchewan Museum in 1967, approximately 20 km south of Shaunavon, Saskatchewan on the east side of Hwy 37. The skull lacks a major portion of the right squamosal, which may have resulted from an injury pre mortem (Fig. 2.9; Tanke and Rothschild, 2002). The left jugal, quadratojugal, and quadrate were also not preserved. Basal skull length is 97 cm, slightly larger than average compared to the other FF material. The nasal horncore of RSM P1163.4 is flat and narrows distally on the dorsal edge. It points anteriorly with a slight posterior curve, traits strongly associated with *T. prorsus* (Scannella et al., 2014). The nasal process of the premaxilla is wide and vertically oriented, another *T. prorsus* trait (Scannella et al., 2014). The postorbital horncores are oriented vertically at an angle of less than 20° from vertical and are missing the apices, though they have been reconstructed with the last 10 cm beginning to point posteriorly (Tokaryk, 1986). Both postorbital horncores are oval in cross-section (Fig 2.9). The frontoparietal foramen is completely closed, indicative of a mature specimen (Horner and Goodwin, 2006). The frill is thick and sulcate with all the epi-ossifications fully fused to both the frill and to each other at their margins, making differentiating and counting them difficult. There does appear to be some thinning of the left parietal; however, no fenestrae are present. There is a large and obvious fracture on the dorsal side of the parietal bar, which has previously been assumed to indicate a healed fracture (Tanke and Rothschild, 2002).

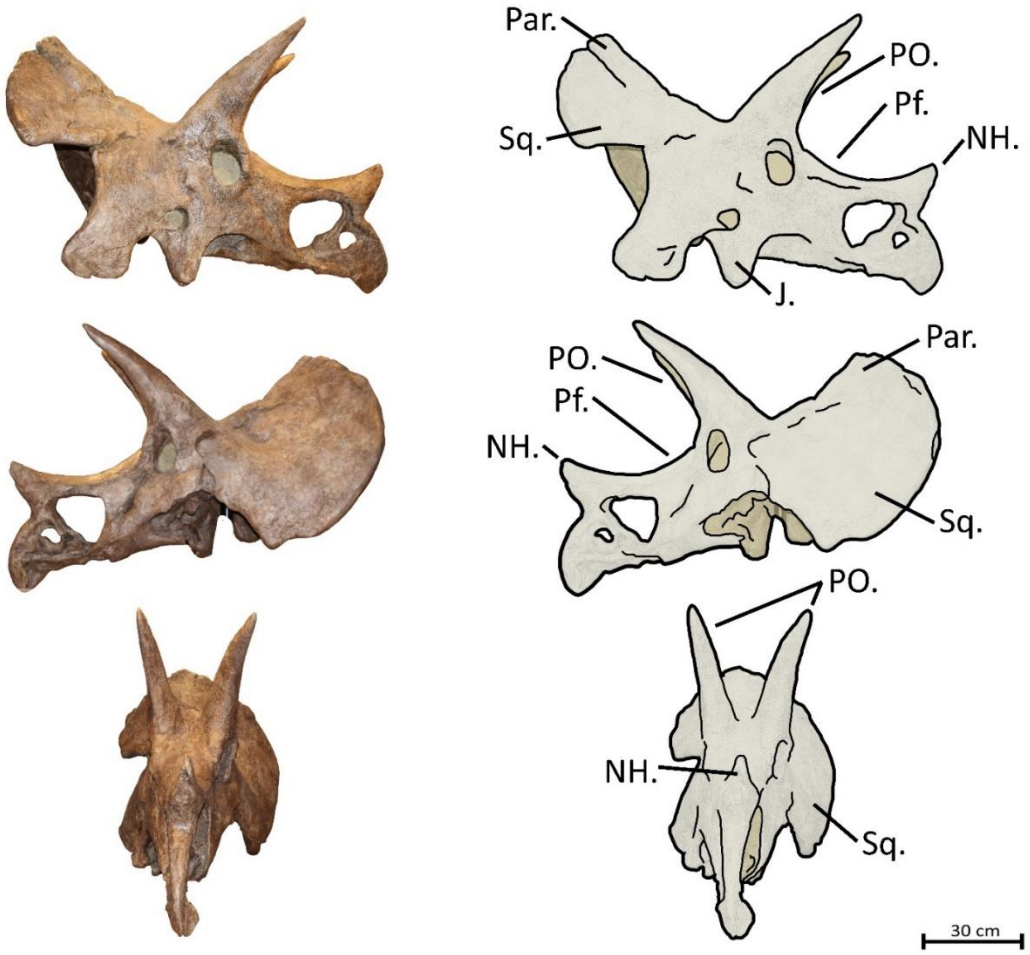

Figure 2.9: Skull of RSM P1163.4 in right lateral (top), left lateral (middle) and anterior (bottom) views. Photographs (left) and line drawings (right) with labeled features Abbreviations: J., jugal, NH., nasal horncore, Par., parietal, Pf., prefrontal bone, PO., postorbital horncores, Sq., squamosal.

RSM P2982.1

RSM P2982.1 is an immature skull found by McGill University in 2007 within the Frenchman Formation of Chambery Coulee, Saskatchewan. It consists of the nasal horncore still attached to the anterior portion of the premaxilla, as well as of fragmentary pieces of the left squamosal, prefrontal, postorbital horncore, dentary, and both jugals (Fig. 2.10). Estimated basal skull length is approximately 55 cm, making it smaller than all the included Frenchman material considered here. The nasal horncore points anteriorly with a slight dorsal ridge, typically traits associated with *T. prorsus*. It has been previously hypothesized that the distinctive posterior curve of the nasal horncore occurs later in ontogeny, indicative of the juvenile nature of RSM P2982.1 (Horner and Goodwin, 2006). The nasal process of the premaxilla is wide and vertically oriented, typical of *T. prorsus.* The postorbital horncores curve anteriorly, a trait typically seen later in ontogeny (Horner and Goodwin, 2006). While the frill is fragmentary in nature, there is enough present to indicate little presence of sulci. There are few to no epi-ossifications preserved, suggesting incomplete fusion resulting in their subsequent loss prior to fossilization.

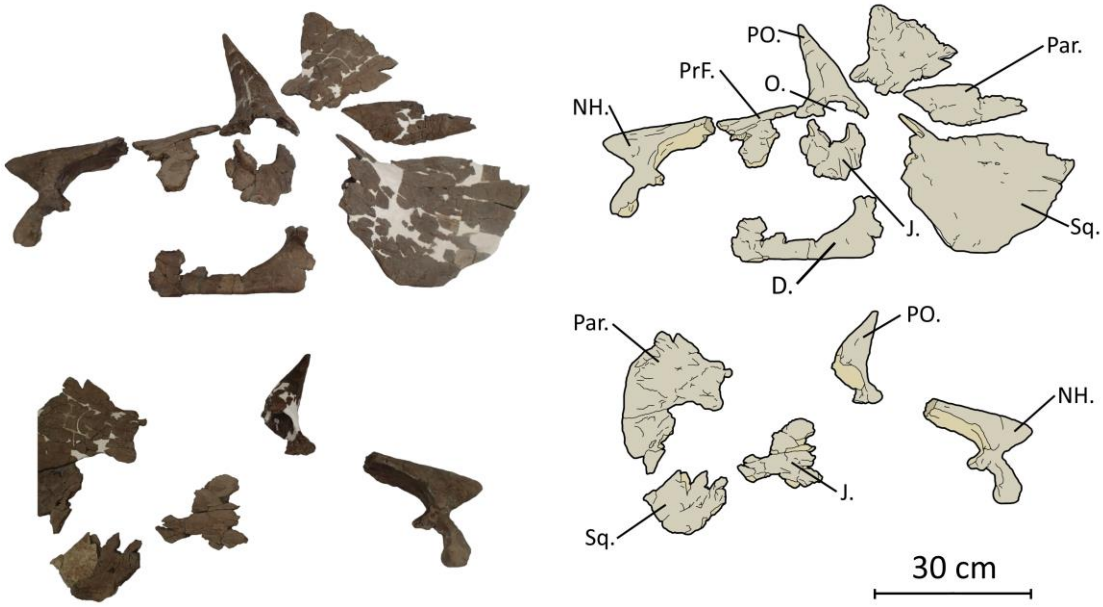

Figure 2.10: Skull of RSM P2982.1 in left lateral (above) and right lateral (below) views. Photographs (left) and line drawings (right) with labeled features. Abbreviations: D., dentary J., jugal, NH., nasal horncore, O., orbit, Par., parietal, PO., postorbital horncores, Prf., prefrontal bone, Sq., squamosal.

Ordination Results

The results for principal component Analysis 1 (PCA1, Fig. 2.11) resulted in a differential clustering of both *T. prorsus* and *T. horridus* across principle component 1 (PC1) with most of the Frenchman material overlapping with *T. prorsus*. Both nasal horncore and postorbital horncore length loaded most heavily on PC1 and PC2, respectively (Table 2.3). Linear discriminate Analysis 1 (LDA1) using the first seven PC scores, which accounted for >90% of the total variation, resulted in four of the unidentified *Triceratops* grouping within *T. prorsus* and two (CMN 8741 and RSM P2982.1) grouping within *T. horridus* (Table 2.6). PC1 and PC7 load heavily on LDA1, indicating that nasal horncore length is the primary variable that differentiates *T. horridus* and *T. prorsus.*

Within PCA2 (Fig. 2.12), *T. horridus* and *T. prorsus* did not overlap throughout PC1, instead only being differentiated across PC2 with the Frenchman material overlapping with *T. prorsus* on PC2. Variable 1 and 4, both measures of nasal horncore length, loaded most heavily on PC2. LDA2, using the first six PC scores which accounted for > 90% of the total variation, resulted in five of the unidentified *Triceratops* grouping with *T. prorsus* and one (CMN 56508) grouping with *T. horridus* (Table 2.6).

Finally, in PCA3 (table 2.5), *T. horridus* and *T. prorsus* are only notably differentiated across PC1, with variables 2 and 4, measuring the length and orientation of the nasal horncore, loading heavily on PC1. LDA3 using the first six PC scores, accounting for >90% of the variation, loaded most heavily on PC1,

resulting in all six unidentified *Triceratops* grouping with *T. prorsus* (table 2.6). PC2 and PC6, where variables that measure the length and orientation of the postorbital horncore loaded heavily, also negatively loaded heavily on LDA3, indicating that increasing nasal horncore size was associated with decreasing postorbital horncore size.

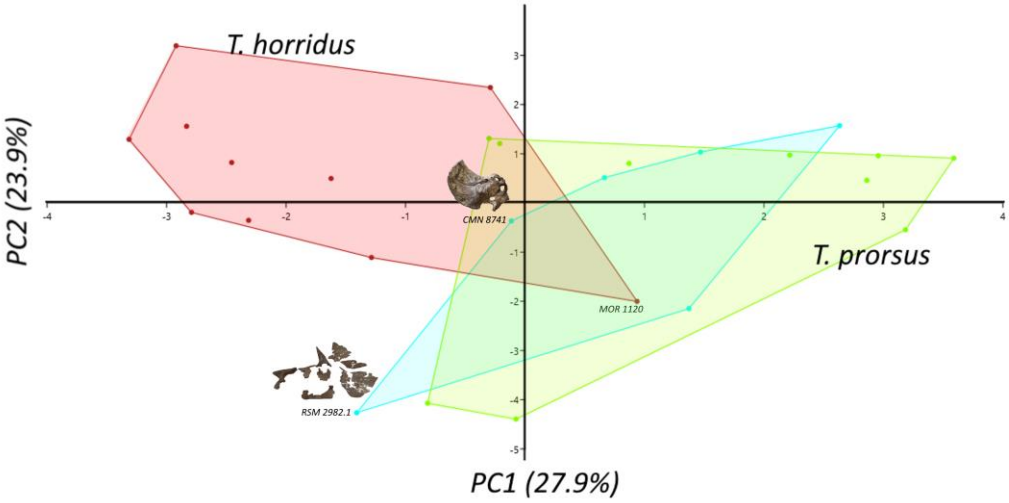

Figure 2.11: Principal Component Analysis 1 showing relationship between PC1 and PC2 created using a subset of variables that were present in at least 50% of all specimens. Red represents *T. horridus* specimens, green represents *T. prorsus* specimens, and blue represents material from the Frenchman Formation. Both RSM 2982.1 and CMN 8741 are highlighted as they were both unexpectedly classified as *T. horridus* in the Linear Discriminant Analysis.

Table 2.3: Summary of PCA and LDA results for Analysis 1, which includes only variables present in at least 50% of the dataset.

Principal component	Amount of variation accounted for (%)	Heavily loading variables	LDA loadings
PC1	27.9	2, 3, 4, 6, 18, 27	1.1453
PC2	23.9	5, 7, 28, 29	-0.21826
PC3	11.2	28, 29	0.088485
PC4	9.57	8	0.94914
PC5	7.17	9, 21	0.73741
PC6	6.32	9	0.0036031
PC7	4.3	2, 3	1.2218

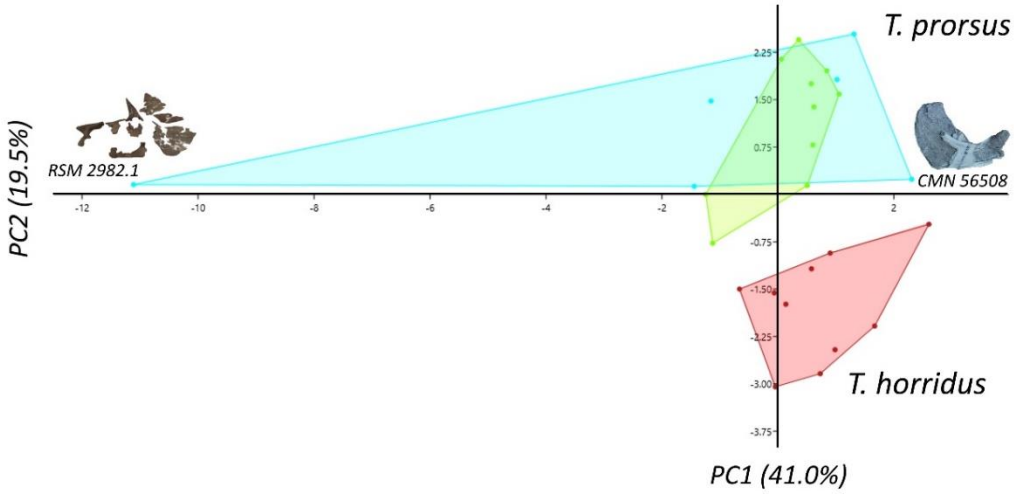

Figure 2.12: Principal component analysis 2 showing relationship between PC1 and PC2, created using a subset of variables that were present in at least 50% of all Canadian specimens. Red represents *T. horridus* specimens, green represents *T. prorsus* specimens, and blue represents material from the Frenchman Formation. CMN 56508 is highlighted as it was unexpectedly classified as *T. horridus* in the linear discriminant analysis. RSM 2982.1 is highlighted due to it being an outlier.

Table 2.4: PCA and LDA results for Analysis 2 which includes only variables which are present in at least 50% of the Canadian material.

Principal component	Amount of variation accounted for (%)	Heavily loading variables	LDA loadings
PC1	41.0	9, 12-17, 22	-0.66554
PC2	19.5	1,4	1.3949
PC3	12.2	7,8	-0.05177
PC4	8.5	11	0.57397
PC5	5.5	8	-0.10488
PC6	3.8	9, 16	0.13637

Table 2.5: PCA and LDA results for Analysis 3, which includes only variables considered diagnostic of *Triceratops spp*.

Principal component	Amount of variation accounted for (%)	Heavily loading variables	LDA loadings
PC1	31.5	2,4,10	2.1187
PC2	23.6	5,7,15	-1.28120.6921
PC3	12.8	3,4	0.5499521573
PC4	9.7	9	0.4464617989
PC5	7.2	8	-0.3518816869
PC6	5.7	7, 15	-1.5617

Table 2.6: Linear discriminant analysis classification results of three separate datasets. Green represents LDA classification of *T. prorsus*, while red represents classification of *T. horridus.*

Specimen ID	**Analysis 1** **Only variables which are present in at least 50% of the dataset**	**Analysis 2** **Only variables which are present in at least 50% of the Canadian material**	**Analysis 3** **Only variables considered diagnostic characters**
RSM 2982.1	*T. horridus*	*T. prorsus*	*T. prorsus*
CMN 8741	*T. horridus*	*T. prorsus*	*T. prorsus*
CMN 56508	*T. prorsus*	*T. horridus*	*T. prorsus*
EM P15.1	*T. prorsus*	*T. prorsus*	*T. prorsus*
RSM P1163.4	*T. prorsus*	*T. prorsus*	*T. prorsus*
CMN 34824	*T. prorsus*	*T. prorsus*	*T. prorsus*

Cluster Analysis Results

Cluster Analysis 1 (Fig. 2.13) resulted in a majority of the *T. horridus* specimens grouping together, with a few outliers falling out independently. However, YPM 1821, a *T. horridus* specimen, grouped centrally within *T. prorsus*. Additionally, a majority of the *T. prorsus* grouped together when using the same limit distance. If a smaller limit distance is considered, *T. prorsus* was subdivided into two groups, with most of the HCF specimens grouping together. When considering the Frenchman material, all but two specimens (CMN 34824 and RSM P2982.1) grouped together.

Cluster Analysis 2 (Fig. 2.14) resulted in three *T. horridus* groups with a majority of *T. horridus* grouping together, and two individuals (DMNH 48617 and MOR 1120) falling out separately. Nearly all the *T. prorsus* specimens grouped together except three: YPM 1822 and YPM 1823, which grouped together, and RSM P2982.1, which fell out alone.

Cluster Analysis 3 (Fig 2.15) resulted in all but two *T. horridus* (DMNH 48617 and MOR 1120) grouping together. All *T. prorsus* grouped together except three (RSM P2982.1, YPM 1822, and YPM 1823), which formed a secondary grouping.

Across all three cluster analyses, two *T. horridus* (DMNH 48617 and MOR 1120) consistently appeared as individuals. Additionally, two *T. prorsus*, YPM 1822 and YPM 1823, regularly grouped together but were outside the main *T. prorsus* cluster. A majority of the *T. prorsus* from the Hell Creek Formation

also grouped together, and formed distinct clusters when the distance limit was decreased.

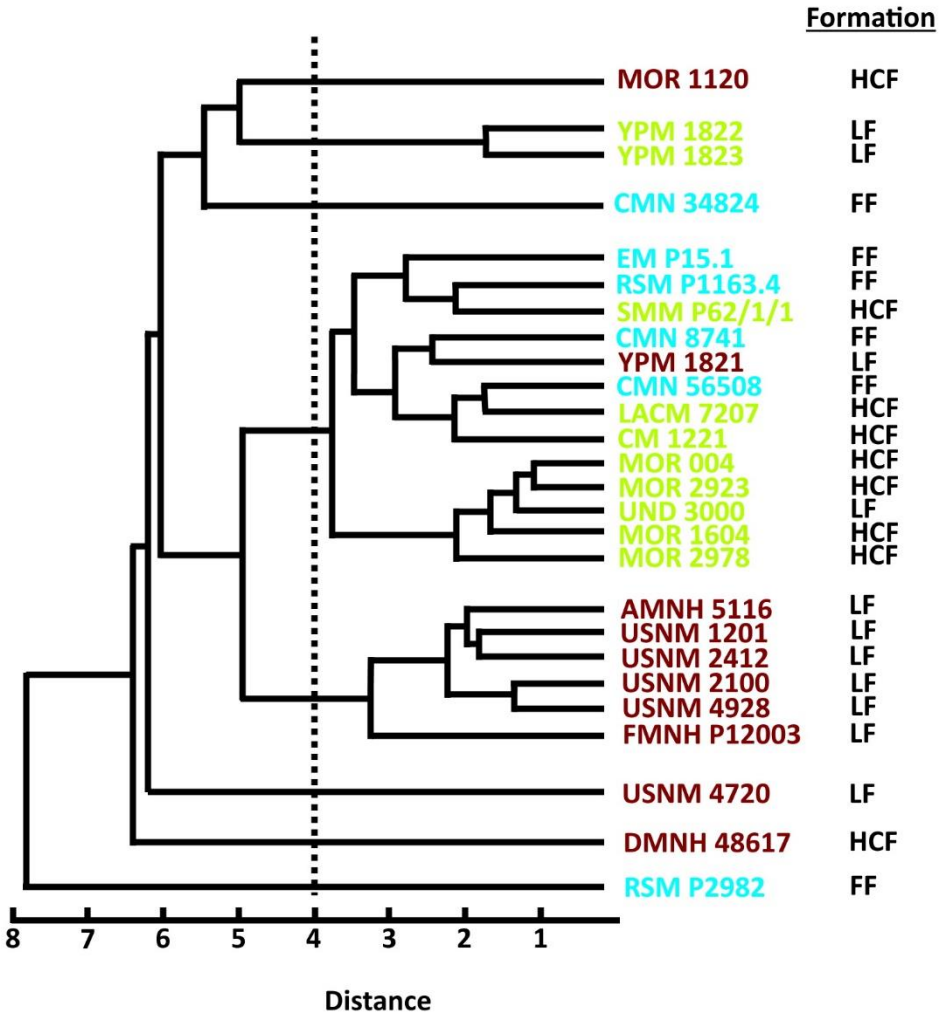

Figure 2.13: Cluster Analysis 1 using all variables which are present in at least 50% of the dataset. Red represents *T. horridus*, green represents *T. prorsus*, and blue represents the Frenchman material. A distance limit of 4 was set as it best separates *T. prorsus* from *T. horridus*. Abbreviations: FF, Frenchman Formation, HCF. Hell Creek Formation, LF. Lance Formation.

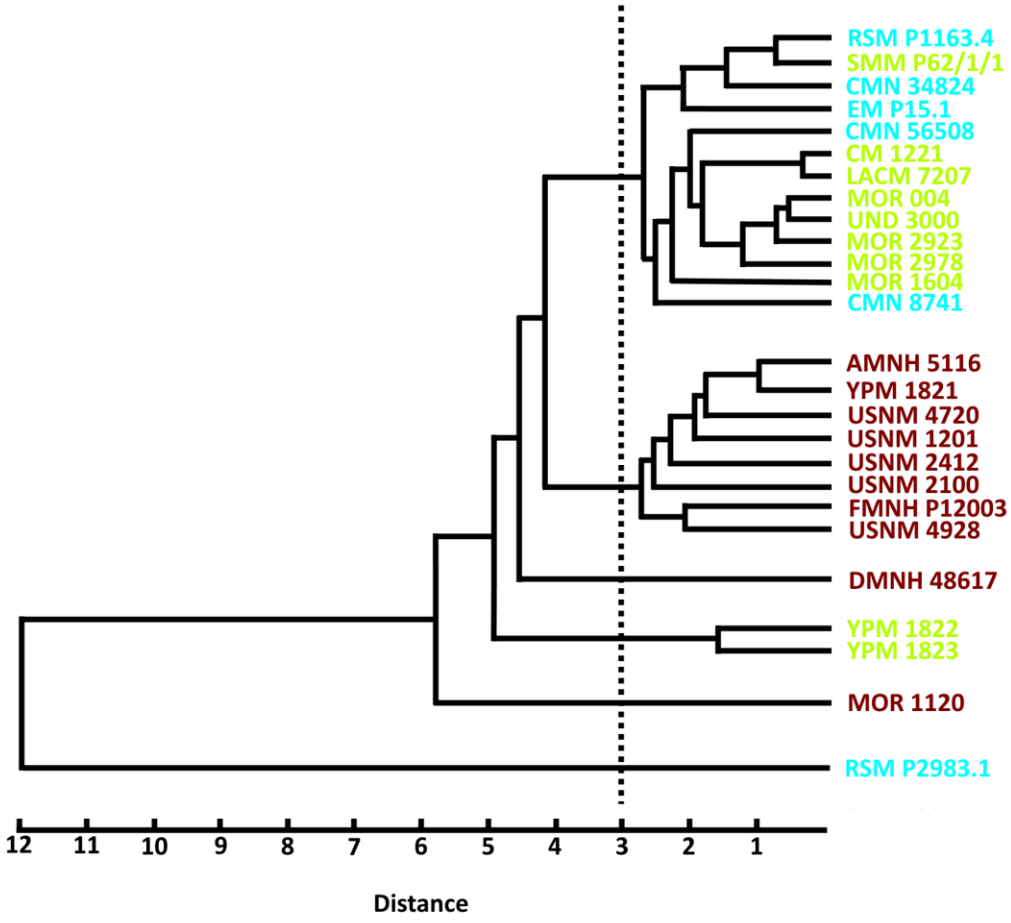

Figure 2.14: Cluster Analysis 2 using all variables which are present in at least 50% of the Canadian material. Red represents *T. horridus*, green represents *T. prorsus*, and blue represents the Frenchman material. A distance limit of 3 was set as it best separates *T. prorsus* from *T. horridus*. Abbreviations: FF, Frenchman Formation, HCF, Hell Creek Formation, LF, Lance Formation.

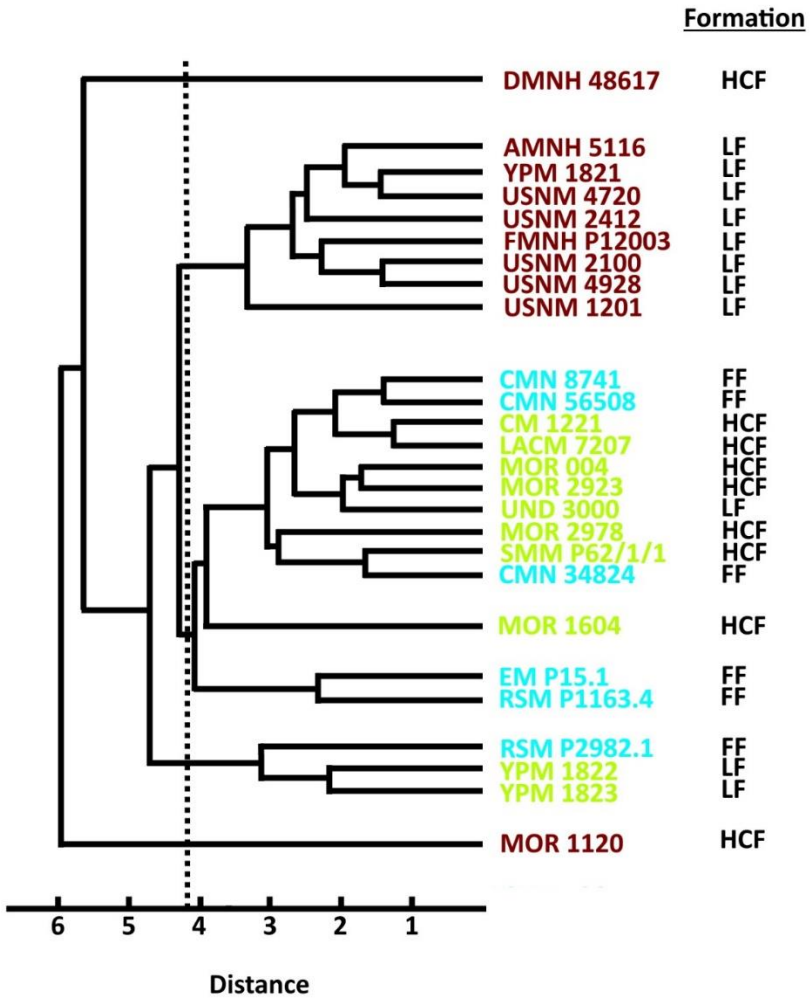

Figure 2.15: Cluster Analysis 3 using all variables considered diagnostic of *Triceratops spp*. Red represents *T. horridus*, green represents *T. prorsus*, and blue represents the Frenchman material. A distance limit of 3 was set as it best separates *T. prorsus* from *T. horridus*. Abbreviations: FF, Frenchman Formation, HCF, Hell Creek Formation, LF, Lance Formation.

Discussion

If the anagenesis hypothesis is true, then all specimens found within the Frenchman Formation must be classified within *T. prorsus* (Fig 1.3). Based on qualitative descriptions, all the Frenchman specimens appear to share more traits with *T. prorsus* than with *T. horridus*. Previously, Scannella et al. (2014) noted that some specimens from the upper middle section of the HCF exhibited mixed traits of both *T. horridus* and *T. prorsus*, providing support for a gradual species turnover, typical of anagenesis. While no strong qualitative *T. horridus* characters appear within the Frenchman material, some FF specimens may display morphology closer to these "transitional" specimens which may provide an explanation for the material occasionally being classifed as *T. horridus* within various sub analyses.

The linear discriminant analysis resulted in most of the Frenchman material grouping with *T. prorsus,* with only a few outliers. In analysis 1, RSM 2982.1 is classified as *T. horridus*; however, qualitatively this specimen has a nasal horncore and accompanying nasal process of the premaxilla that is diagnostically *T. prorsus* (Fig. 2.10). The nasal process of the premaxilla points vertically and is wide and robust in RSM 2982.1. Additionally, RSM 2982.1 is both comparably smaller and fragmentary compared to the rest of the Frenchman material. Its fragmentary nature likely impacted the imputations, as even those variables that were measured were partially estimated. Furthermore, the immature

nature of RSM 2982.1 could impact the classification of the specimen, as derived *T. prorsus* characters would be more pronounced later in ontogeny.

CMN 8741 was also classified as *T. horridus* in LDA 1; however, 75% of the variables were imputed for this specimen within this analysis, which increases the likelihood of errors. While most of the key diagnostic characters are missing, CMN 8741 does have a strongly convex squamosal, a trait usually associated with *T. prorsus* (Scannella et al., 2014). Additionally, when comparing PC1 and PC2 (which collectively accounts for 53.8% of the total variation) CMN 8741 overlaps with both *T. horridus* and *T. prorsus* (Fig. 2.11).

CMN 56508 was also classified as *T. horridus* in LDA 2 using a subset of data that included all variables present within >50% of the Canadian material (Fig. 2.12). While CMN 56508 does group with *T. horridus* along PC1, 65% of all specimens overlap along PC1 (which has high loading scores associated with frill size and face shape), suggesting there is little notable differentiation other than size across the axis. This suggests that CMN 56508 could be falling outside the *T. prorsus* grouping in PC1 because it is an atypically large *T. prorsus* specimen. Also of note is RSM 2982.1, which is a major outlier on PC1, yet it still classified as *T. prorsus*. The reasoning behind its huge differentiation is due primarily to its size. For perspective, the average length of the squamosal, measured from the parietal-squamosal contact at caudal frill margin to the ventral most edge of squamosal, across the entire dataset is 85 cm. However, RSM 2982.1 has a squamosal length of only 38 cm, less than half the average.

Although the LDA occasionally classifies specimens as *T. horridus*, each specimen is classified as *T. prorsus* in at least two of the three analyses. Therefore, the majority of the LDA evidence weighs in favour of the *T. prorsus* interpretation for the Frenchman material.

Additionally, the cluster analyses consistently groups most of the Frenchman material within *T. prorsus*. RSM 2982.1 remains a persistent outlier, grouping within neither species cluster, likely due to its comparably smaller size. This suggests that anacladogenesis is unlikely to be the evolutionary mode that characterizes the evolution of *Triceratops* during the end-Cretaceous.

Within the cluster analyses, some inconsistent grouping within *T. prorsus* did appear. Cluster analysis 1 (Fig 2.13) revealed that much of the Hell Creek material clustered together, with a majority of the other *T. prorsus* specimens forming a sister group. While the Hell Creek material does cluster closely in the other cluster analyses, the resolution is not as strong and distinct groups cannot be distinguished (Fig 2.14;2.15). Therefore, while some evidence exists that there may be a differentiation between the *T. prorsus* of the Frenchman and those from the Hell Creek, it is not strong enough to support a cladogenetic event having occurred between them.

These findings agree with the previous identification of a much smaller subset of the material all being classified as *T. prorsus* (Tokaryk, 1986). Additionally, the lack of any consistent species grouping found in the cluster analysis also supports the previous anagenesis hypothesis (Scannella et al, 2014). Because the Frenchman material is contemporaneous in time but differs spatially

(up to 1000 km apart) from some of the American material, support for population-wide anagenesis comes with some inherent ecological implications. For anagenesis to occur, the entire population needs to be genetically homogenous. Any isolated population could have been subject to either genetic drift or natural selection, or both, resulting in said population's divergent evolution. Previous studies have supported estimates of only 50,000 to 100,000 years for those diverging punctuated equilibrium events to take place (Ayala, 2005). As the FF lasted for 840,000 years (Eberth & Kamo, 2019), and *T. prorsus* specimens are found throughout 73% of the formation (the youngest being approximately 27m below the K-Pg boundary), there would have been ample time for an isolated population to diverge if any long-term isolation had occurred. Additionally, since *Triceratops* fossils are so common, large population sizes can be inferred, which would also limit the effects of genetic drift. If environmental pressures are constant, and the population stays large, evolutionary stasis can occur over long periods of time (Bakhtin et al. 2020). As only one species of *Triceratops* is present within the FF population, we can support the hypothesis that an anagenetic event took place within *Triceratops* prior to the FF deposition, with the population remaining in evolutionary stasis until their extinction.

However, one caveat that should be addressed is that there may simply not be enough variation preserved in the fragmentary Frenchman material to differentiate within groups of *T. prorsus*, causing the false rejection of the cladogenesis hypothesis. Nevertheless, while small sample sizes and incomplete

specimens may bias the results, the material present still largely supports anagenesis.

Conclusion

The results of both the LDA and cluster analysis support that the Frenchman material should all be classified as *Triceratops prorsus*. While some specimens did classify as *T. horridus* in select analyses, said outliers still classified as *T. prorsus* in most cases. Additionally, while *T. prorsus* and *T. horridus* consistently clustered apart in all cluster analyses, no repeatable differentiations between subpopulations of *T. prorsus* were evident. Therefore, we can reject both alternative hypotheses of cladogenesis and anacladogenesis and find further support for the previous hypothesis that anagenesis occurred within *Triceratop*s.

Chapter 3: Evolutionary tempo at the end of the Cretaceous

Introduction

The mass extinction event at the end of the Cretaceous Period marked the end of the non-avian dinosaurs, and allowed for the rapid radiation of mammals, eventually leading to the evolution of our own species (Halliday et al., 2016; Grossnickle and Newham, 2016). The best explanation for this event comes from the Yucatán Peninsula impact crater and the associated global iridium ash layer, which support a large extraterrestrial impact occurring roughly 66 million years ago (Alvarez et al., 1980). Said impact would have set off a chain reaction of global cataclysms, evidence for which is widespread (Schulte et al., 2010; Schoene et al., 2019; Chiarenza et al, 2020). However, the end-Cretaceous prior to the impact event was already in a state of environmental upheaval as a result of changing global sea levels, cooling climates, massive volcanic activity, and the rapid radiation of other clades like flowering plants and mammals (Miller et al., 2005; Coiffard et al., 2012; Magallón et al., 2015; Grossnickle & Newham, 2016; Grasby et al., 2019; Condamine et al., 2021). Consequently, there is much debate regarding the evolutionary tempo and mode of dinosaurs immediately prior to their extinction.

For many years, the prevailing thought was that non-avian dinosaur diversity exhibited a decreasing trend throughout the end-Cretaceous, leading to their ultimate extinction (Russel, 1984). Recently, more support for the diversity decrease was proposed when Sakamoto et al. (2016) used a time calibrated phylogeny to support a general diversity decline, with dinosaur extinction rates exceeding speciation rates well before the K-Pg extinction event. Furthermore, Condamine et al., (2021) estimated both preservation rates and diversification and diversity metrics of North American dinosaurs and suggested that the diversity decreases seen prior to the K-Pg event could have been driven by global climate cooling resulting in herbivorous dinosaur diversity decreases, which subsequently cascaded through the food chain.

However, there is still no consensus on whether dinosaurs were in decline or not prior to their extinction. Many argue that any decline in dinosaur species richness or ecological diversity seen during the last million years of the Cretaceous is simply a result of a biased or incomplete fossil record (Benton et al., 2000; Brusatte et al., 2015; Chiarenza et al., 2020). Attempts have been made to better impute the missing data (Silvestro, 2019), however these methods rarely consider preservation biases within specific intervals of geological space and time (Close et al., 2020; Condamine et al., 2021).

If dinosaur diversity in the end-Cretaceous was decreasing then we might expect to see that reflected not only in species richness counts, but also in the tempo and mode of species evolution. The previous chapter supported a slow and gradual anagenetic shift between the two accepted species of *Triceratops*.

However, while *Triceratops prorsus* had completely replaced *Triceratops horridus* by the latest Cretaceous, it is not known if *T. prorsus* was still undergoing directional change or was in a state of evolutionary stasis prior to its extinction. If *T. prorsus* was in a state of stasis, then that implies that either there was an exhaustion of beneficial variations within the population, or that said variations were unable to spread across the entire species ranges, both of which imply a decrease in species diversity (Eldredge et al., 2005).

However, because *Triceratops* had a vast range, expanding from Western Canada to New Mexico, it becomes necessary to explore not only species wide evolution but also to take a regional approach, as the small-scale evolutionary trends arising within a sub population may not be present or strong enough to spread over the entire range. While some work to this extent has been completed within the Hell Creek Formation of Montana (Scanella et al., 2014), further research into additional *Triceratops* specimens from other formations is required to obtain the larger picture.

The *Triceratops* found in both the Scollard and Frenchman formations of Canada represent the northern-most limit of the genus's range and as such would have been the most likely area for selection to occur since range limits are typically areas of increased genetic isolation, genetic differentiation, and individual variation (Sexton et al, 2009; Nadeau & Urban, 2019). Therefore, this chapter will attempt to stratigraphically relate several specimens of *T. prorsus* from the Frenchman Formation, placing them in geochronological order to detect if any small scale evolutionary patterns exist or if the population was in

evolutionary stasis. Additionally, the depositional environments of the Frenchman Formation will also be documented and compared to other *Triceratops*-bearing units to determine whether any trends present. Since previous studies have found that *Triceratops* remains are most often found in mudstone deposits (Lyson and Longrich, 2011; Scanella and Fowler, 2014), the depositional environments of the FF should be considered to ensure that any differences are not representative of different habitats.

Geological Background of the Frenchman Formation

Surface exposures of the Frenchman Formation occur throughout southern Saskatchewan (Fig 3.1), with contemporaneous deposits in Alberta (Scollard Formation), Montana, North Dakota, and South Dakota (Hell Creek Formation), and Wyoming (Lance Formation) (Johnson et al., 2001; Lehman et al., 2006; Richardson, 2008). The depositional environment of the FF was fluvial in nature, with sediments accumulating along a coastal plain bordering the Western Interior Seaway (Horner et al., 1992; Fowler, 2020). The Upper Cretaceous beds of southern Saskatchewan represent a period of drastic environmental change attributed to regression-transgression cycles, which is evident across consecutive formations.

Figure 3.1: Regional geology map of uppermost exposed strata in Saskatchewan, including a general location of fossil quarry localities (Chambery coulee and Grasslands national park). Based on geological maps from Dawson et al, 1994.

The geological succession of Maastrichtian-aged southern Saskatchewan sediments begins with the Bearpaw Shale (equivalent to the much thicker Pierre Shale of Manitoba), a predominantly marine shale which thins westward and is composed of dark grey silty clays (Kaykun, 2008). The Bearpaw Shale coarsens upwards and is gradationally overlain by the Eastend Formation (He et al., 2005).

The Eastend Formation, made primarily of uniform, fine-grained sandstones, is representative of lagoonal, tidal, and shallow marine depositional environments. The Eastend Formation grades into the kaolinized clays of the Whitemud Formation, which appear stark white in colour when heavily eroded and are representative of in-situ sediment leaching when exposed above sea level (Byers, 1969; McIver, 2002; Lerbekmo, 2009). The top of the formation represents a period of sea level decrease, exposing and subjecting the surface to regionally varying levels of erosion (Fraser et al, 1935; Sweet et al, 1997; McIver, 2002).

The overlying Battle Formation is a thin layer of bentonitic sediments, indicative of a period of intense volcanism, cool temperatures, and low sediment input in the basin (Eberth & Kamo, 2019). The formation is organic-rich and often representative of estuarine channel and tidal flat environments (Fowler, 2020). The top of the Battle Formation, where it meets the overlying FF, is defined by an unconformity. In many areas, differentiation between the Battle and Frenchman formations is difficult, leading previous studies to combine both into a single unit (McIver, 2002).

The youngest of the Maastrichtian sediments within southern Saskatchewan, the FF, is made primarily of horizontal rocks, consisting largely of fluvial deposits that are continuous with the overlying Ravenscrag Formation but are separated by the Ferris coal seam. Within the Ferris coal seam, an iridium-rich clay layer signifying K-Pg boundary marks the limit of the non-avian dinosaurs.

The FF is composed of two usually distinct sand and clay facies (Kupsch, 1956, 1957; McIver, 2002), which can be divided into broader sandstone and mudstone units that cycle through fining upward sequences (Bamforth, 2014; Bourque et al, 2021). The lower sand facies consists of laterally discontinuous, loosely consolidated, fine-grained sandstones that range in colour from greenish-grey to yellowish-orange and brown, with medium- scale cross stratification (Kupsch, 1956). The sand facies may also contain clay and silt lenses, and in some areas, it is common for iron rich sandstones to become cemented by calcium carbonate, forming large sandstone masses (Kupsch, 1956). The upper clay facies are composed mostly of grey to green bentonitic clays, which create the iconic popcorn-like texture when the weathered surface is dry (Kupsch, 1956; Kolaceke et al, 2018).

Additional fossil evidence points towards the FF representing a fluvial depositional setting, with both plant and animal remains adapted to riparian regimes. Fossils include aquatically adapted crocodiles, champsosaurs, turtles, and fish, as well as lizards, snakes, a few birds, and at least 14 terrestrial dinosaur species (Tokaryk, 1997; McIver, 2002; Redman et al, 2015). Several dozen groups of plants have also been identified within the FF, including angiosperms,

gymnosperms and cycads (Bamforth, 2014). The presence of palm fruit and semi-tropical to tropical fauna such as crocodiles, suggests that the region was mesothermal and that freezing temperatures were rare. Additionally, leaf margin analyses have resulted in subtropical climate estimates characterized by warm temperatures and a defined seasonality (McIver, 2002; Bamforth, 2014). The region was most likely dominated by open-canopied, swampy to lowland forests of deciduous conifers with diverse angiosperm assemblages comprising the mid-canopy and understory (Bamforth, 2014). Furthermore, large masses of hardened calcareous ironstone and paleosols with evidence of frequent wildfires suggest that the region was seasonally dry (Bamforth, 2014).

Dating and Correlating the Frenchman Formation

Determining the presence of fine scale evolutionary trends requires accurate and reliable dating metrics. Typically, this can be done through lithostratigraphic correlations across multiple localities containing like species. However, fluvial deposits, like those found in the FF, are generally laterally consistent over only a few kilometers at best, making traditional lithostratigraphic correlations difficult (Fowler, 2020).

Based on abundant radioisotopic, palynostratigraphic, and sequence data, the most recent estimates date the Frenchman Formation within a range of 66.88–66.04 Ma (Eberth & Kamo, 2019). However, the upper third of the contemporaneous HCF probably represents less than 0.3 Myr of time, suggesting

that the FF could also be contemporaneous with at least some higher portions of the middle Hell Creek Formation as well (Sprain et al., 2015). By contrast, magnetostratigraphic estimates place the base of the FF within the uppermost C30n magnetozone, with C29r making up the remaining formation, resulting in the FF being equivalent solely to the upper HCF (Lerbekmo, 1999; Lerbekmo and Braman, 2002; Eberth & Kamo, 2019).

Luckily, the K-Pg boundary acts as a key stratigraphic indicator within the Frenchman Formation. The K-Pg boundary is present across most of the exposed formation and occurs at the base of the Ferris coal seam or slightly above. It is composed of a thin layer of tonstein, a sedimentary rock composed of kaolinite clay, thought to be related to the fallout from the Chicxulub impact at the end of the Cretaceous (Alvarez et al., 1980; Smit and Hertogen, 1980). Below the K-Pg boundary, the fossil fauna is dominated by dinosaurs, whereas above the K-Pg boundary no non-avian dinosaurs are found and instead the fauna is dominated by small mammals (Brown, 1907). Using this boundary as a datum, it should be possible to determine the relative age of each *Triceratops*, which in turn can be used to determine if any evolutionary trends are detectable.

Materials and Methods

Quarry Relocation

The primary purpose of this chapter is to determine if any small-scale evolution can be detected within the Canadian *Triceratops*. This requires the relative age for each specimen be known which requires corresponding stratigraphic data. Unfortunately, while the FF has produced a number of excellent *Triceratops* specimens dating back to the early 1920s, a general emphasis at that time was given to the collection of exhibit quality specimens, with limited regard given to the precise documentation of location and stratigraphic position of the material. This lack of information therefore requires the relocation and documentation of each *Triceratops* quarry before the material can be placed in relative sequence and the evolution of *Triceratops* in Canada evaluated. Such quarry relocation programs have proven successful elsewhere, such as in Dinosaur Provincial Park in Alberta (Tanke, 2005; Tanke and Evans, 2014).

Using original field notes at the Canadian Museum of Nature and the Royal Saskatchewan Museum, approximate locations were obtained for several of the more complete *Triceratops* skulls. These locations were often recorded as legal subdivision (LSD) descriptions, which can be used to describe an area of approximately 0.25 mi^2 (= 0.65 km^2). Using the legal land descriptions in conjunction with more precise descriptions of the local geology, and historical photographs taken at the site (when available), the original locations of the

Triceratops quarries could then be found. Once an approximate location was determined, field investigations began by traveling to the determined location and looking for signs of human activity. Quarry debris, such as wooden planks and old bits of plaster (used in field jacketing), were used to confirm the location of sites, and then matched with field descriptions and photos (when available). Once found, GPS co-ordinates, further site descriptions, and photographs were taken for posterity. Using these methods, two previously unknown sites were located, CMN 56508 during the 2019 field season and a possible location for CMN 8741 during the 2020 season. These, combined with the four more recent sites with well documented locations, resulted in a total of six locations for this study (summarized in Table 3.1).

Because of issues of low topography, slumping, and the generally overgrown nature of the FF where it crops out, it was necessary to create composite sections by following unit boundaries to better exposures nearby (within ~ 100 m). Frequently, digging with a pick and shovel was required to clearly expose the section. Newly exposed faces were at least 30 cm in width to ensure that enough of the unit was exposed to reveal any structures within. The final exposure was cleared using a hand trowel to preserve any delicate features that might have been present. Section thickness was determined using a Jacob's staff, measured to the nearest 2.5 cm. The thickness of each layer, primary lithology, grain size, colour, and any sedimentary structures were recorded.

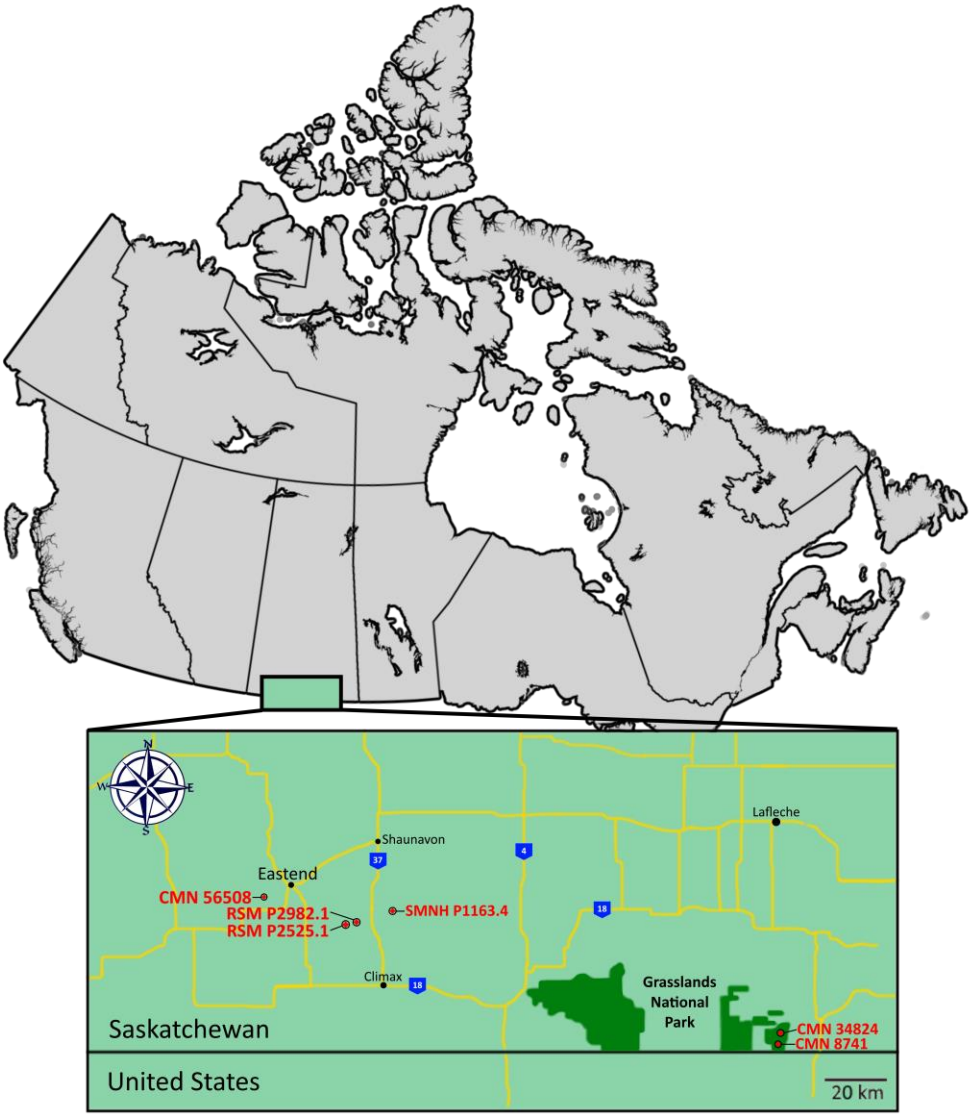

Figure 3.2: Site locations of six *Triceratops* quarries showing their spatial relationship to each other.

PCA and Regression

To detect any morphological trends among *Triceratops* specimens, a principal component analysis (PCA), which is a method of multivariate discrimination of shape, was done. Principal component analysis is designed to analyze sets of correlated variables, in this case derived from linear distance measurements taken from *Triceratops* skulls. However, as covered in Chapter 2, the preserved nature of many of the Canadian *Triceratops* material presented a problem when determining which variables to use to detect variation amongst them. Because principal component analyses require a complete dataset, the imputed datasets used in the second chapter were used (imputed using Bayesian principal component analysis in R v 4.0 (R Core Team, 2020) using the package pca Methods (Stacklies et al, 2007)). For each of the three datasets, a PCA was run in PAST v 4.03 (Hammer et al., 2001). Because all the specimens from the FF were classified as *T. prorsus* within the previous chapter, three additional *T. prorsus* from the nearby HCF with associated depth measurements below the KPg were added using published datasets (Scannella et al., 2014) to better encapsulate any directional change that had occurred at the end-Cretaceous. An ordinary least squares regression was then applied, fitting the scores of each principal component against their relative age onto a linear model to detect the presence of any trends in shape change over time were present. Plots were created in R v 4.0 (R Core Team, 2020) using the packages ggplot2 (Wickham, 2016) and ggrepel (Slowikowski et al, 2021). Because sample sizes were so small, a simple linear model was chosen to avoid overfitting. To better visualize if stasis had occurred

each specimen was connected chronologically with a dotted line, and the PC score mean was plotted vertically.

Finally, to determine if any correlation between deposit type (mud vs sand) and PC score existed, a Point Biserial Coefficient analysis (PBCA) was competed in R v 4.0 (R Core Team, 2020). A PBCA measures the strength of association between a continuous variable and a binary variable, and ranges from 0 to 1, where 0 is no relationship and 1 is a perfect relationship (Sheskin, 2011).

Results

Stratigraphic Profiles

A total of six quarries were mapped and sectioned (summarized in table 3.1). Within five of the stratigraphic sections, the Ferris coal seam was present, allowing for the creation of a combined section map summarizing the trends of *Triceratops* deposition within the Frenchman Formation (Fig. 3.4). While the Ferris coal seam was absent within the CMN 8741 section, an approximate distance from the top of the underlying Eastend Formation, combined with a generalized section map for the surrounding Grasslands National Park, allowed an estimated depth in relation to the other sites to be made (Bamforth et al., 2014).

Table 3.1: Summary of *Triceratops* quarries used in study, with locations, depositional sediment type and depth below K-Pg.

Specimen ID	Quarry locations	Primary sediment type at quarry	Depth below Ferris coal Seam (m)
CMN 8741	eastern block of Grasslands National Park	Loosely consolidated, cross-bedded sandstone	~ 27
CMN 34824	eastern block of Grasslands National Park	Mudstone	16.05
RSM P2982.1	Within Chambery Coulee, west of Hwy 37	Loosely consolidated sandstone	9.2
RSM P2525.1	Within Chambery Coulee, west of Hwy 37	Mudstone	10.25
CMN 56508	east of Hwy 37, ~25 km south of Shaunavon	Mudstone	4.3
SMNH P1163.4	~10 km west of Eastend	Loosely consolidated sandstone	13

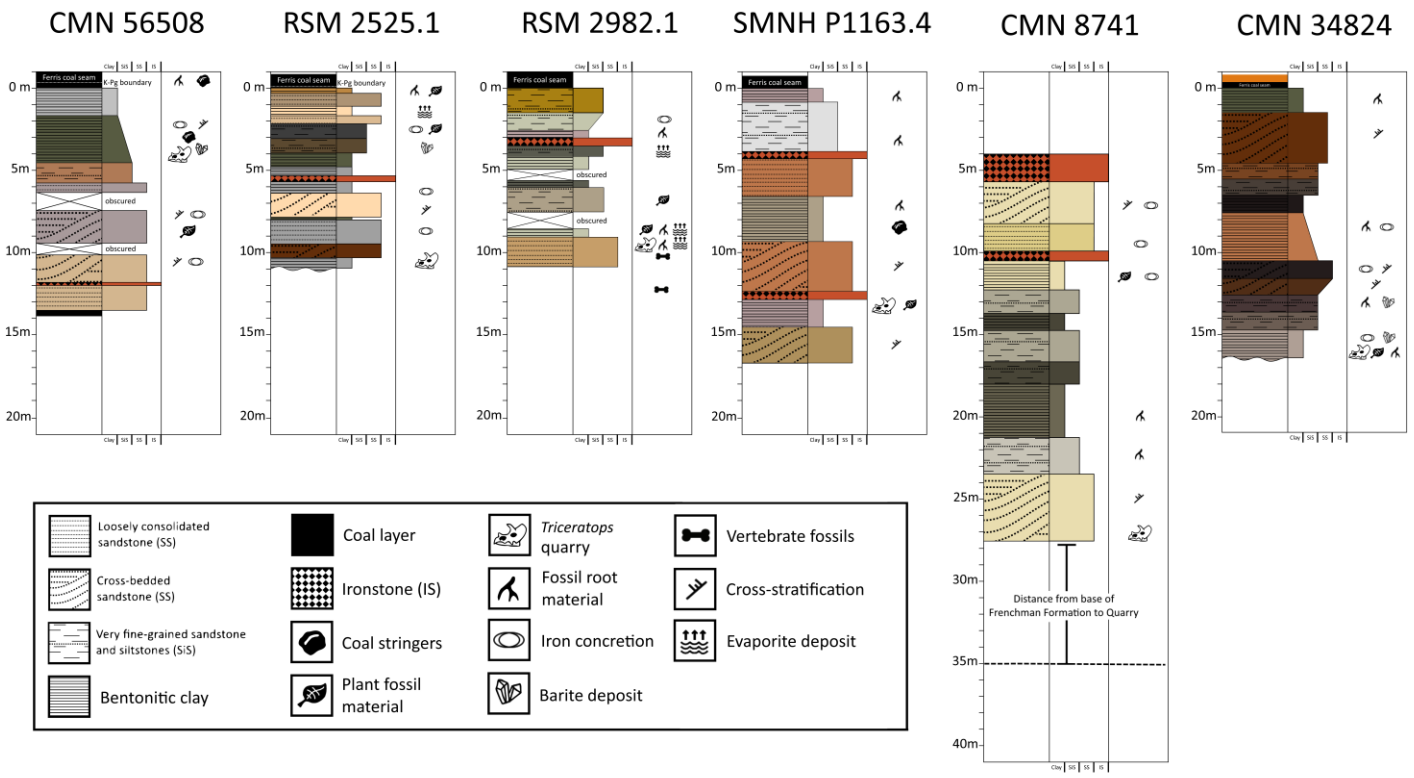

Figure 3.3: Stratigraphic charts of southern Saskatchewan *Triceratop*s quarries scaled to each other with the bottom of the Ferris coal seam standardized at 0 m. Individual charts correspond to individual specimen quarries located West to East. For chart five (CMN 8741), the Ferris coal seam was absent, so distance was measured from the base of the Frenchman Formation, and checked against a generalized stratigraphic chart for Grassland National Park (Bamforth et al., 2014).

Correlation of Depth vs PC Scores

The results of the first linear regression, which measured the first six PC scores (representing >85% of the total variance) of Analysis 1 against depth below the K-Pg boundary resulted in no significant trends being present (Fig. 3.4, Table 3.2). In each case, the trendlines repeatedly wobbled across the mean resulting in no accumulated change being detected throughout the end-Cretaceous.

The second linear regression, which measured the first six PC scores (representing >85% of the total variance) of Analysis 2 against relative age, also resulted in no significant overall trends being present among any of the plotted graphs (Fig. 3.5, Table 3.3).

Finally, when plotting PCA 3 scores against depth below the K-Pg boundary using the first six PC scores (accounting for >90% of the variance), no significant trends were apparent (Fig. 3.6, Table 3.4).

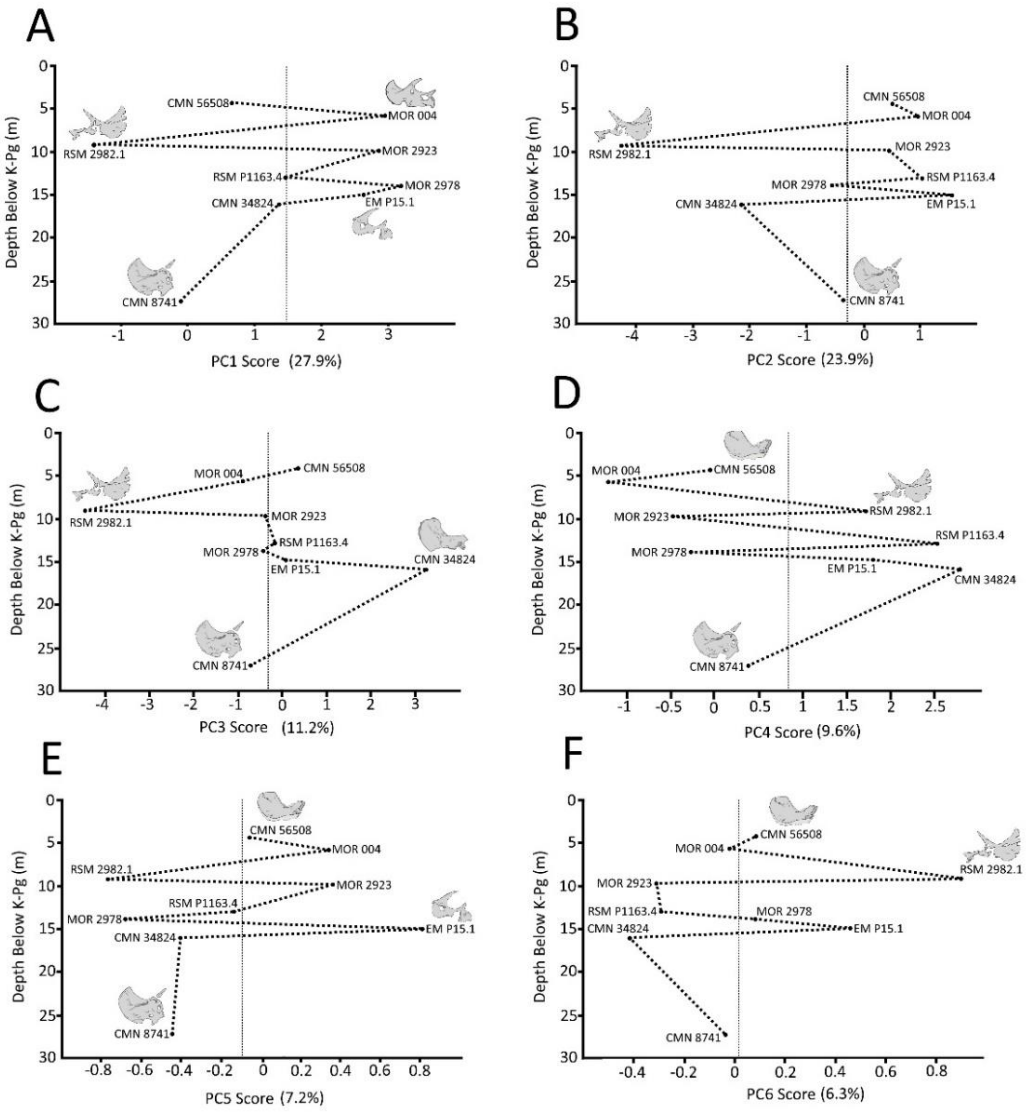

Figure 3.4: Plot of *Triceratops* principal component scores (with associated variation each score accounts for) against age of fossil deposition showing no significant trends in morphology. A through F represent the first six PC scores from PCA 1 (imputed using only variables present in at least 50% of the specimens) in sequential order. Dotted lines joining each specimen emphasises morphological change over time, while the vertical dashed line indicates the mean of each PC score.

Table 3.2: Summary of linear regression statistics, comparing PCA 1 scores against relative age

Plot	R-squared	F-statistic	p-value
A	0.001	0.003	0.960
B	0.007	0.028	0.874
C	0.037	0.098	0.770
D	0.001	0.0001	0.992
E	0.095	0.023	0.887
F	0.010	0.014	0.910

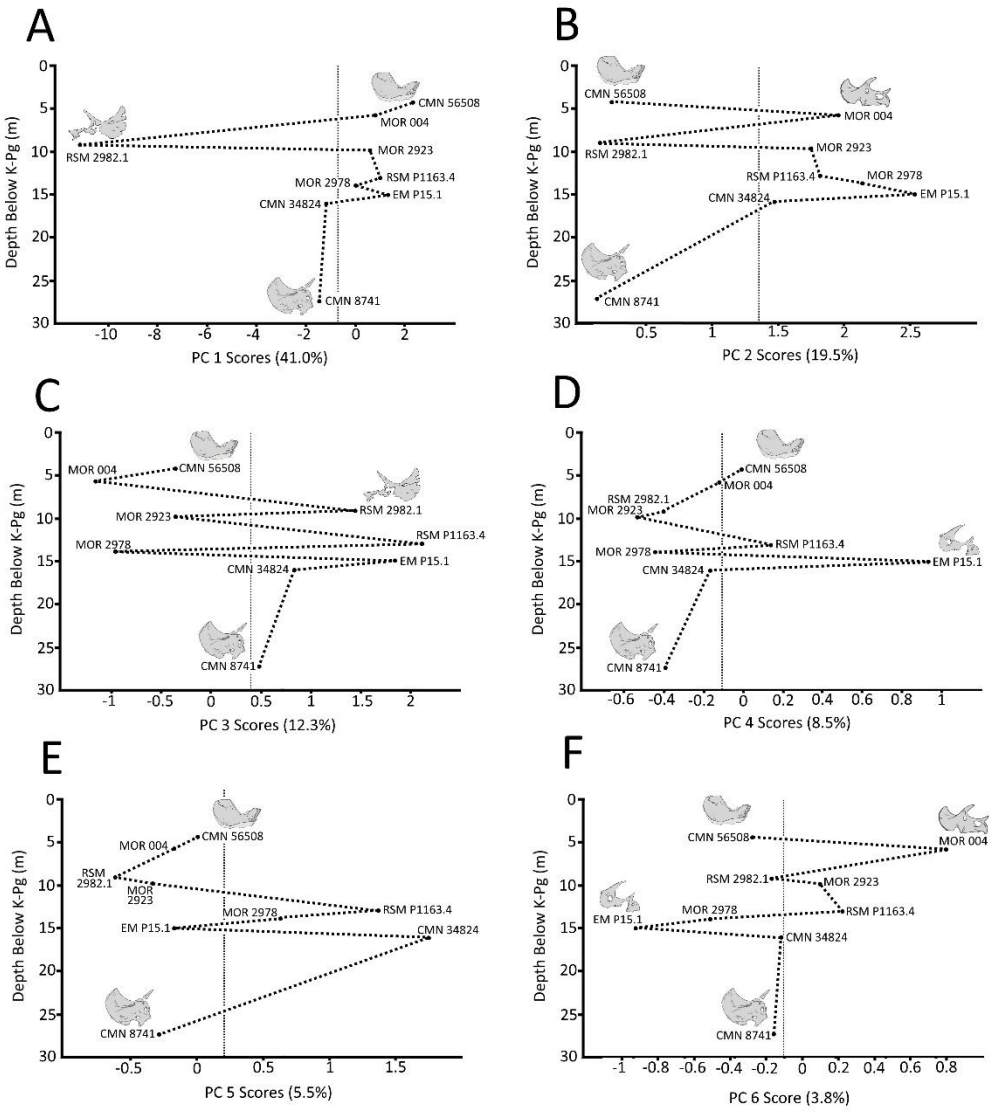

Figure 3.5: Plot of *Triceratops* principal component scores (with associated variation each score accounts for) against age of fossil deposition showing no significant trends in morphology. A through F represent the first six PC scores from PCA 2 (imputed using only variables present in at least 50% of the Canadian specimens) in sequential order. Dotted lines joining each specimen emphasises morphological change over time, while the vertical dashed line indicates the mean of each PC score.

Table 3.3: Summary of linear regression statistics, comparing PCA 2 scores against relative age

Plot	R-squared	F-statistic	p-value
A	0.003	0.013	0.916
B	0.0004	0.002	0.970
C	0.007	0.029	0.873
D	0.024	0.097	0.771
E	0.0001	0.001	0.983
F	0.0002	0.001	0.979

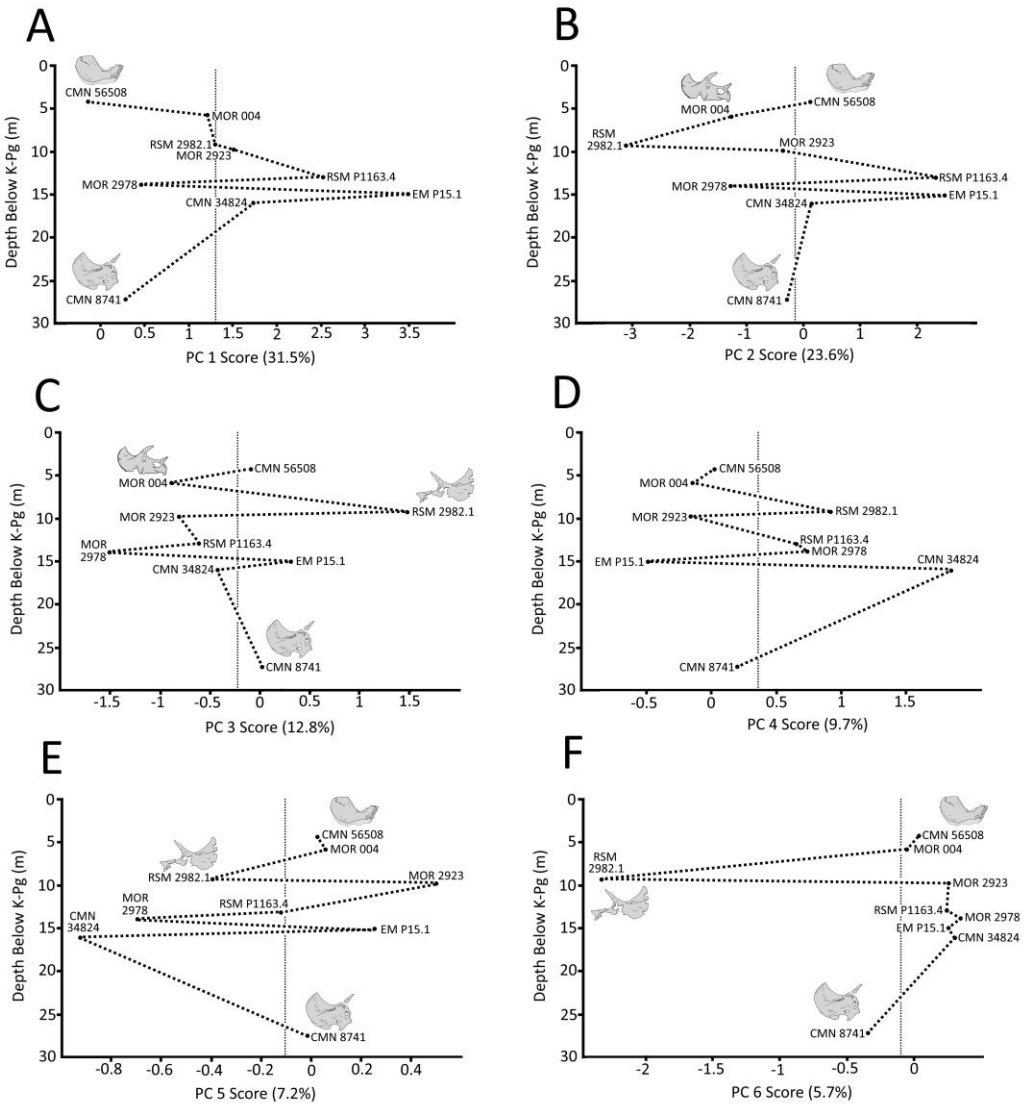

Figure 3.6: Plot of *Triceratops* principal component scores (with associated variation each score accounts for) against age of fossil deposition showing no significant trends in morphology. A through F represent the first six PC scores from PCA 3 (imputed using diagnostic variables differentiating *T. prorsus* and *T. horridus*) in sequential order. Dotted lines joining each specimen emphasises morphological change over time, while the vertical dashed line indicates the mean of each PC score.

Table 3.4: Summary of linear regression statistics, comparing PCA 3 scores against relative age

Plot	R-squared	F-statistic	p-value
A	0.0004	0.002	0.969
B	0.015	0.060	0.819
C	0.289	0.171	0.701
D	8.03e-08	3.21e-07	0.100
E	0.253	0.0012	0.974
F	0.030	0.125	0.741

Correlation of Depositional Environment and PC Scores

Depositional environments were recorded for nine *T. prorsus* specimens, three found within sand dominated facies, with the remaining six found in clay dominated facies. The three specimens from the HCF were all deposited within clay dominated facies. Within the FF, the six specimens were equally distributed between the two sediment types. Specimens deposited within sand facies were not confined temporally, being found throughout the Frenchman Formation. Point-biserial correlation analyses were run using the first six PC Scores of all three data subsets against the sediment type with only one statistically significant result. PC 1 within PCA 1 resulted in a significant difference between PC scores and depositional environments, but was not repeated when run with different data subsets.

Table 3.5: Comparing depositional environments and principal component scores from PCA 1 (a subset of variables which included all measurements present in at least 50% of *Triceratops* specimens) using a point-biserial correlation analysis.

PC Score	point-biserial correlation coefficient	p - value
PC1	-0.729	0.026 *
PC2	-0.361	0.340
PC3	-0.537	0.136
PC4	0.389	0.301
PC5	-0.483	0.187
PC6	0.252	0.514

Table 3.6: Comparing depositional environment and principal component scores from PCA 2 (a subset of variables which included all measurements present in at least 50% of *Triceratops* specimens from the Frenchman Formation) using a point-biserial correlation analysis.

PC Score	point-biserial correlation coefficient	p - value
PC1	-0.559	0.117
PC2	0.528	0.144
PC3	0.567	0.112
PC4	-0.178	0.646
PC5	-0.078	0.841
PC6	0.126	0.746

Table 3.7: Comparing depositional environment and principal component scores from PCA 3 (a subset of variables which included all measurements considered diagnostic to *Triceratops prorsus*) using a point-biserial correlation analysis.

PC Score	point-biserial correlation coefficient	p - value
PC1	-0.006	0.988
PC2	-0.095	0.808
PC3	0.508	0.163
PC4	0.199	0.608
PC5	-0.049	0.899
PC6	-0.587	0.096

Discussion

Regional Trends in *Triceratops* Evolution

When comparing the PC scores of *T. prorsus* against their stratigraphic position (measured as the distance each specimen was deposited below the K-Pg boundary), no significant trends were found (Fig 3.4 -3.6). Rather it would seem that PC scores wobble repeatedly across a central mean, implying a general plasticity in *Triceratops* morphology, but without any directional change. Therefore, *T. prorsus* was likely in a state of evolutionary stasis leading up to their extinction at the end of the Cretaceous.

To be considered a speciation event within the fossil record, a novel phenotype must first originate, become established within a population, and then disburse in large numbers across the entire population (Eldredge et al., 2005). The wobble seen in the PC scores might be interpreted as the repeated origination of new phenotypes, however none become established, resulting in the overall stasis seen within the species. Alternatively, the wobble may just be representative of natural plasticity, which may be apparent should a larger sample size fill in the gaps between the outlying PC scores.

In the previous chapter, further support for an anagenetic event occurring between the *T. horridus* found in geologically older formations and *T. prorsus* was found within the FF. While anagenesis is usually associated with gradualism (the slow accumulation of traits over time), evolutionary stasis is typically associated with a punctuated equilibrium event, which usually occurs rapidly after a cladogenetic event (Rhodes, 1983; Brett et al., 1996). It is possible that anagenesis was still occurring through evolutionary gradualism but that there is simply not enough information or geological time recorded to detect any morphological differences. This

would agree with previous findings that support the slow and gradual replacement of *T. horridus* with *T. prorsus* (Scannella et al., 2014). Additionally, the existence of specimens that display a mix of traits from both *T. horridus* and *T. prorsus,* such as those found within the middle HCF, point toward a gradual transition.

A possible explanation for the evolutionary stasis seen within *T. prorsus* could be due to the co-evolution between both *Triceratops* species and that of its main predator *Tyrannosaurus rex*. Typically, it is assumed that co-evolutionary process such as those described in the Red Queen hypothesis increase speciation rates, however mathematical models have indicated that geographic structure can constrain the escalation of antagonistic arms races (Eldredge et al., 2005). These continual interactions between predator and prey across both large population sizes and geographical areas can result in the continuous recycling of novel traits, resulting in lack of new polymorphisms which frequency dependent selection requires (Gandon et al. 1996; Gomulkiewicz et al. 2000; Nuismer et al. 2000; Eldredge et al., 2005). This could explain the wobble seen, where each outlying PC score would represent a novel trait, unable to establish itself within the population as a whole, resulting in overall stasis of the species. Recently, support that *Tyrannosaurus rex* was comprised of three species (*T. rex*, *T. regina* and *T. imperator*) was suggested, which could support the co-evolutionary relationship between *Triceratops* and *Tyrannosaurus* (Paul et al, 2022). However, there is not a complete vertical/temporal separation between the different morphs of *Tyrannosaurus* like that found in *Triceratops.* Therefore, further work would be required to determine if this hypothesis could be supported.

Alternatively, while unlikely, a cladogenetic event could have occurred between *T. horridus* and *T. prorsus*, with one or more ghost lineages existing contemporaneously with *T. prorsus*. Stasis commonly occurs after a punctuated event, which could have occurred

concurrently with the middle HCF. However, this would require an explanation for the transitional specimens found in the middle HCF. While this hypothesis is currently unsupported, a general caveat of science suggests that any new discovery would require a reassessment. However, given the vast sampling effort of the HCF over the last two decades, it is a reasonable assumption to exclude that possibility at this time.

If we accept that stasis is the dominant tempo of evolution seen within the *Triceratops* of the FF, that implies that a stabilization or decrease in the diversity of the genus occurred during the very end of the Cretaceous prior to the K-Pg event. While species diversity may have decreased, recent studies have shown that prolonged periods of stasis, increase genetic diversity (Arroyave et al., 2019; Sudasinghe, et al., 2021). If the species diversity decreases seen at the end-Cretaceous are true and not a bias in fossil preservation or collection, then an increase in genetic diversity would be expected as it would provide the remaining species with a buffer against extinction. It would be beneficial if future studies were to expand this project to include other groups of Late Cretaceous dinosaurs to determine if stasis was the norm, or if something unique had occurred within *Triceratops*.

Trends in Depositional Environments

Another caveat to consider when discussing the evolutionary tempo of the FF *Triceratops* is whether the Saskatchewan specimens represented a typical *Triceratops*, or if the population preserved there was somehow unique. While there is a general lack of material when compared to other *Triceratops*-bearing units such as the HCF, this may be due to a lesser collecting effort through time, and the lesser area of exposure of the strata (Scannella and Fowler, 2014).

When comparing the depositional environments of *Triceratops* deposits, several previous studies found that *Triceratops* fossils were dominantly associated with clay or mudstone facies (Lyson and Longrich, 2011; Scanella and Fowler, 2014; Fowler, 2020). Lyson and Longrich compared the depositional environments of North American dinosaur families, and found that Ceratopsidae (n=161) were nearly twice as likely to be found in mudstone deposits than in sandstone. A 2014 survey on *Triceratops* localities in the HCF listed 19 specimens being found in clay deposits in addition to mentions of numerus uncatalogued fragmentary specimens, while *Triceratops* deposited within sand-dominated facies were rare, with only five specimens noted (Scanella and Fowler, 2014). Lyson and Longrich offered an ecological interpretation suggesting that niche partitioning was occurring, with *ceratopsians* primarily occupying floodplains, while other large herbivores, such as Hadrosaurs and Thescelosaurus, occupied the sand-dominated river margins.

However, these patterns could also be interpreted as taxon preferences for varying basin drainage regimes, differing in sediment accommodation settings and causing changes to the proximity of the shoreline and environments (Fowler, 2020). The sand dominated facies were deposited during periods of low sediment accommodation, where well drained floodplains and

stable shorelines would have created inland environments. Alternatively, when the levels of groundwater rose, creating high-accommodation settings, mudstone facies would have been deposited in the more poorly drained, swampy environments. Rather than river and flood plain niche partitioning, *Triceratops* being found largely in clay-dominated mudstone facies may have been representative of their preference for swampy coastland environments (Brinkman et al., 1998).

Nevertheless, while these depositional patterns have been shown before, mostly within the HCF, when compared to the Frenchman material, a subtle difference appears. The *Triceratops* quarries that were relocated within the FF were equally distributed between both sand and clay facies, with three individuals found in each. While this is likely due to small sample sizes, it warrants mention for future investigation.

When comparing various PC scores, representative of *Triceratops* skull measurements, and the depositional sediment type each specimen was found in, little to no significant correlations existed. One PC score, which had high loading scores for nasal horn and frill length, significantly differentiated between specimens deposited within clay and sand facies, however those significance levels disappeared when the test was rerun using different subsets of imputed data. Furthermore, differences in habitat preference due to ontogeny can be rejected as both SMNH P1163.4, one of the largest specimens, and RSM P2982.1, the smallest specimen in this study, were both found within sand dominated facies. Additionally, if ontogeny was a determining factor, any PC score that had high loadings for size should strongly differentiate specimens based on depositional type, which they do not.

Ultimately, I do not believe that the *Triceratops* from the FF differ significantly from

those found in the adjacent HCF, and that any differences are simply artifacts of small sample size.

Conclusion

The results of the linear regression support that *T. prorsus* were most likely in a state of evolutionary stasis prior to their extinction at the end of the Cretaceous. I found little to no significant support that any trends in morphology existed; rather, PC scores tended to wobble repeatedly across a mean, indicative of species level stasis. We found no correlation between depositional environment and morphology, and while more of the Frenchman material was found within sand-dominated facies than expected when compared to other *Triceratops*-bearing units, this was likely a sampling bias and would correct itself if more specimens were added to the dataset.

Chapter 4: Conclusions and future work

Summary of Thesis

Previous work in the Hell Creek Formation found that two species of *Triceratop*s are stratigraphically separated, with *Triceratops horridus* found lower in section and *Triceratop*s *prorsus* isolated to the upper third. This, in addition to a few speculative "transitional" specimens found within the middle HCF, led to the hypothesis that an anagenetic shift occurred between them (Scannella et al., 2014). This study focused on expanding this hypothesis to include material from the Frenchman Formation of southern Saskatchewan, representative of the species' northern range limit.

Because the FF is contemporary with the upper third of the Hell Creek Formation, for the anagenesis hypothesis to remain true, all specimens must be *T. prorsus*. Two alternative hypotheses—anacladogenesis and cladogenesis—were also tested. The first requires that both *T. prorsus* and *T. horridus* were contemporaneous; the second requires either distinct subpopulations of *T. prorsus* or the existence of a third species of *Triceratops* altogether.

Based on new qualitative descriptions of *Triceratops* from the Frenchman Formation, all material classified as *T. prorsus*. This agrees with previous descriptions (Tokaryk, 1986) and provides further support for an anagenetic shift between *T. prorsus* and *T. horridus*. Furthermore, linear discriminant analyses, conducted using various subsets of skull measurements, resulted in a majority of specimens classifying as *T. prorsus*. Those that classified as *T. horridus* were discounted because they were immature or heavily imputed. Therefore, because no definitive examples of *T. horridus* were found, the alternative anacladogenesis hypothesis can be rejected.

The subsequent cluster analysis resulted in no distinguishable groups existing between the *T. prorsus* found in the Frenchman and those found in any other formation. Consequently, the second alternative hypothesis of cladogenesis can also be rejected.

As was common in early palaeontology, little associated stratigraphic information was collected with the *Triceratops* specimens from the Frenchman Formation. This project aimed to help rectify this shortcoming by relocating and collecting stratigraphic information at six *Triceratops* quarries from across southern Saskatchewan. The resulting stratigraphic profiles matched those previously done for other Frenchman localities (Kupsch, 1956; Bamforth, 2014; Fowler, 2017) in that the profiles showed repeating facies of fine sandstone and clay.

Using the K-Pg boundary as a datum, the depth of each quarry was recorded and used to date *Triceratops* specimens relative to one another. Those depths were compared against various PCA scores of linear *Triceratops* skull measurements using linear regression; however, no significant trends emerged. Rather, *Triceratops* morphology appeared to "wobble" about a central mean, suggesting that *Triceratops* may have been in evolutionary stasis prior to their extinction at the end of the Cretaceous. Additionally, while more *Triceratops* were found within sandstone deposits within the FF than expected, the general depositional trend follows those seen in other *Triceratops*-bearing units.

Limitations of Current Study

Small sample size is arguably the most limiting factor in any palaeontological study. The effect of small sample size includes reducing the number and type of analyses that can be performed, reducing the statistical and resolving power of those analyses, and increasing the probability of Type II (false-negative) errors (Brown and Vavrek, 2015). With only six specimens and their associated stratigraphic profiles used, it is possible that morphological trends, which would be well-defined using larger sample sizes, may be undetectable here. Additionally, any outliers are going to weigh more heavily on any statistical analyses in small sample studies.

Secondly, the fragmentary nature of the Frenchman Formation material required varying amounts of imputation. While previous studies have proven that imputations using Bayesian principal component analysis is the best performing estimation method, small sample sizes still have high levels of estimation error (Brown et al., 2012). While I attempted to mitigate this though running multiple analysis on subsets of data, obtaining a larger sample size would decrease the estimation error of the BPCA, therefore increasing prediction reliability.

Thirdly, the limitations of geographic availability remain a problem. This study looked at material from the FF of southern Saskatchewan, in an attempt to represent more of a range limit of *Triceratops*. However, fragmentary material exists from the Scollard Formation which would represent the current Northern most limit of their known range. Additionally, it is unknown if even this would represent the true range limit of *Triceratops* as fossil preservation, and exposure limits the material that is available.

Future Directions

Additional Ceratopsian Considerations

This study found support for an anagenetic shift between *Triceratops horridus* and *Triceratops prorsus*. However, in order to streamline the analyses used, several taxa closely related to *Triceratops* were excluded from analyses that could have phylogenetic implications depending on their evolutionary interpretations.

Firstly, *Torosaurus* has been largely debated within the study of *Triceratops* evolution. Attempts have been made to synonymize *Torosaurus* with *Triceratops*, based on bone and horncore histology analyses, and the purportedly transitional *Nedoceratops* (Scannella and Horner, 2011) yet *Torosaurus* was removed from this study due to the assumption that it was not synonymous. Based on morphological similarities, *Torosaurus* is at the very least a close relative of *Triceratops*. However, where that divergence occurred has implications for the evolutionary mode of *Triceratops*. Because *Torosaurus* fossils are contemporaneous with both *T. horridus* and *T. prorsus*, if a cladogenetic event occurred within *Triceratops*, it must have occurred early, near the first appearance of *T. horridus*. Recently, work has shown that *Torosaurus* from the FF, may represent a unique species (Mallon et al., 2022). However, whether this represents an additional anagenetic shift within *Torosaurus*, or if *Torosaurus* really was synonymous with *Triceratops* and the differences in *Torosaurus* represent diverging ontogenetic end-points of *T. horridus* and *T. prorsus* will require more work.

Secondly, USNM 2412, currently considered its own genus, *Nedoceratops* (Ukrainsky, 2007, 2009), may present some implications for *Triceratops* phylogeny if instead situated within the genus *Triceratops*. Forster (1996) noted the absence of a nasal horncore and the presence of

small fenestrae in the parietal of USNM 2412. It has been suggested that the absence of the nasal horncores could have been the result of a taphonomic loss prior to preservation or could have been lost in vivo (Horner and Goodwin, 2008). The parietal fenestrae in *Nedoceratops* are reminiscent to those found in nearly all Chasmosaurinae except for *Triceratops*, suggesting that the lack of fenestrae is a derived trait in *Triceratops*. While it has also been suggested that *Nedoceratops* may be a sub-adult morph of *Torosaurus* (Scannella and Horner, 2011), it is possible that *Nedoceratops* represents a sub-species of early *T. horridus*, which would imply that cladogenesis, rather than anagenesis, occured within *Triceratops* (Fig 4.1). USNM 2412 has an elongated rostrum and posteriorly oriented nasal process of the premaxilla, characteristics of *T. horridus*, and the presence of small parietal and squamosal fenestrae could represent a regression to the ancestral trait where fenestrae were common or could be pathological in nature. This could initially be tested using a specimen-level stratocladistic analysis, but would require the relocation of the original quarry and the collection of additional stratigraphic information to determine the relative age of *Nedoceratops*.

Finally, a second currently questionable species of *Triceratops* also exists within the Scollard Formation of Alberta, "*Triceratops albertensis*". The holotype skull, CMN 8862, consists primarily of the left cheek and facial region, a partial left postorbital horncore, and a left squamosal. The postorbital horncore is distinctive as it is oriented vertically, slightly posteriorly. Previous descriptions have claimed that this orientation in addition to an enlarged antorbital fossa, is due to severe post-depositional deformation (Ostrom and Wellnhofer, 1986; Forster, 1996). However, the orientation of the postorbital horncore is strikingly similar to that seen in *Nedoceratops*. Additionally, the left squamosal has a medially smoothed indent, which could be interpreted as the lateral edge of a squamosal fenestra, similar to that seen in *Nedoceratops*. If

*Nedoceratop*s and *T. albertensis* are synonymous, either representing ontogenetic stages or natural variation within a single species, then an argument could be made for a cladogenetic event occurring within *T. horridus*, resulting in two sister groups of *T. prorsus* and the *T. albertensis/ Nedoceratops* groups. Future stratocladistic analyses, which again would require associated stratigraphic data, could be used to determine if there was any validity to this hypothesis.

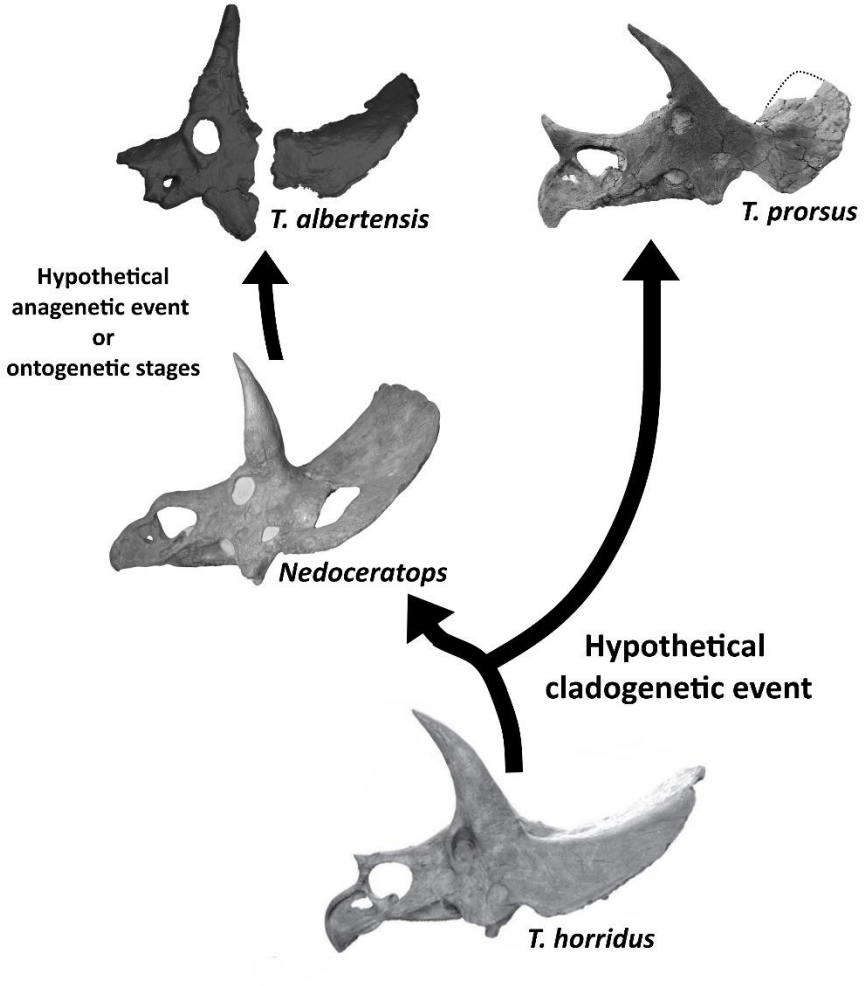

Figure 4.1: Hypothetical phylogeny placing *Nedoceratops hatcheri* (USNM 2412) and *Triceratops albertensis* (CMN 6682) within the genus *Triceratops*.

Additional *Triceratops*-bearing Formations

While this study adds support for anagenesis occurring within the *Triceratops* of both the HCF and the FF (Scannella et al., 2014), their ranges were widespread. *Triceratops* fossils have also been found within the Lance and Evanston formations of Wyoming, the Laramie and Denver formations of Colorado, the Scollard Formation of Alberta (Longrich and Field, 2011), and the McRae Formation of New Mexico (Lucas et al., 1998). Therefore, additional studies should be completed using specimens from these various formations. Any formations that are contemporaneous with the upper HCF and the FF should only contain *T. prorsus*, while any formations contemporaneous with the lower HCF should only contain *T. horridus*. Stratigraphic data are often a limiting factor in paleo-evolutionary studies, because accurate correlations between specimen ages are required. While knowing which formation each specimen came from gives enough resolution for macro-evolutionary phylogenies, proper stratigraphic profiles like those done here and within the Hell Creek surveys (Scannella et al., 2014) should be completed in years to come to determine if *Triceratops* were experiencing regional stasis or if it was population wide.

Additional Considerations Regarding Species Turnover

Anagenesis requires that environmental pressures remain relatively constant, and that no isolation occurs throughout the entire species population (Emerson and Patiño, 2018). Because support for anagenesis was found within the *Triceratops* of the Frenchman Formation, this warrants study into other taxa that lived contemporaneously with *Triceratops* to determine if the faunal turnover was experienced across the entire community. Previously, a gradual decline in diversity during the end Cretaceous of North America had been hypothesized (Sloan et al., 1986;

Sakamoto et al., 2016). Typically, when diversity indices remain either relatively constant or decline, any extinction is going to have a greater affect on the biodiversity of a non-diversifying ecosystem. However, if stasis commonly occurred within many taxa at the end-Cretaceous, then that may have allowed for the buildup of genetic diversity within the reducing number of species. When genetic diversity increases within a population, it provides a buffer, allowing species to rebound quickly in response to environmental changes or disease. Future studies should look at other Frenchman Formation taxa with regards to their relative stratigraphic locations to determine if both anagenesis or evolutionary stasis was the norm at the end Cretaceous, or if what was occurring with *Triceratops* was unique.

Final Remarks

All *Triceratops* observed from the FF of southern Saskatchewan were both qualitatively and quantitatively classified as *T. prorsus*, further supporting that an anagenetic shift occurred between *T. prorsus* and *T. horridus*. No morphologic trends were revealed over time indicating an evolutionary stasis of the species prior to the end-Cretaceous. Although the research presented here elucidates what may have occurred within one group, further study into the evolutionary mode and tempo of contemporaneous FF taxa is need to better understand biodiversity trends prior to the K-Pg extinction.

Appendices

Appendix table 2.1: Descriptions of all linear skull measurements taken with assigned variable numbers. Not all measurements used in analysis as many were incomplete or absent.

Variable	Name	Description
V1	Basal Skull length(cm)	the anteriormost point of the rostrum to the posterior surface of the occipital condyle
V2	nasal horn length (cm)	from tip of nasal horn to nasal-premaxilla contact
V3	Width of nasal (cm)	transverse width of nasals at nasal premaxilla contact
V4	Measurement 4	tip of nasal horn to dorsalmost rim of orbit (average)
V5	circumference of the SOH	circumference of the postorbital horn base (average)
V6	Measurement 6	transverse width from dorsalmost rim of orbit to dorsalmost rim of orbit
V7	Measurement 7	tip of rostral to nasal-premaxilla contact beneath nasal horn (average)
V8	Measurement 8	tip of rostral to premaxilla-maxilla contact at tooth row (average)
V9	Measurement 9	nasal-premaxilla contact beneath nasal horn to premaxilla-maxilla contact at tooth row (average)
V10	Measurement 10	tip of rostral to tip of nasal horn (average
V11	length of NpPM (cm)	maximum length of nasal process of the premaxilla
V12	Measurement 12	dorsalmost rim of orbit to parietal-squamosal contact at caudal frill margin (average)
V13	Orbit Height (cm)	Maximum Height of Orbits (average)
V14	Orbit width (cm)	Maximum Width of orbits (average)
V15	length of post Orbital Horn (cm)	tip of Post Orbital Horn to dorsalmost rim of orbit (Average)
V16	Measurement 16	squamosal-quadratojugal contact at lower temporal fenestra to parietal-squamosal contact at caudal frill margin
V17	Measurement 17	postorbital-jugal contact at orbit to squamosal-quadratojugal contact at lower temporal fenestra
V18	Measurement 18	squamosal-quadratojugal contact at lower temporal fenestra to ventral tip of jugal
V19	Measurement 19	dorsalmost rim of orbit to ventral tip of jugal
V20	Measurement 20	premaxilla-maxilla contact at tooth row to ventral tip of jugal
V21	Measurement 21	premaxilla-maxilla contact at tooth row to dorsalmost rim of orbit

V22	Measurement 22	parietal-squamosal contact at caudal frill margin to ventralmost edge of squamosal
V23	width of nasal process of the premaxilla	Trasverse width of nasal process of the premaxilla
V24	OHC to OHC	distance from tip of Orbital horn core to Orbital horn core
V25	width of parietal (cm)	transverse width from parietal-squamosal contact at caudal frill margin to parietal-squamosal contact at caudal frill margin
V26	width of sqamosal (cm)	transverse width from ventralmost edge of squamosal to ventralmost edge of squamosal
V27	jugal to jugal (cm)	Transverse width from ventral tip of jugal to ventral tip of jugal
V28	height of OC	Width of occipital condyle
V29	width of OC	Height of occipital condyle
V30	width of Ppr	width across doral edge of paroccipital process
V31	width of Ppr	width across ventral edge of paroccipital process
V32	height of of Ppr	Height of paroccipital process

Appendix table 2.2: Summary of all raw measurements (measurements in cm)

Specimen ID	Species	V1	V2	V3	V4	V5	V6	V7
CMN 34824	?		25		90.5			42
EM P15.1	?	154	45	8.7	91.3			66.5
CMN 8741	?							
CMN 56508	?					64		
RSM P2982.1	?		24	9.4	37.7	43.5		
RSM P1163.4	?	164	38	8.5	85	69.5	39	59
AMNH 5116	*T. horridus*		15	10.8	30	56	49	
FMNH P12003	*T. horridus*		11.3	11.5		84	54	54
MOR 1120	*T. horridus*	156.5	10	6.4	57.5		30	34
USNM 1201	*T. horridus*		12.1	12.5		71		41
USNM 2100	*T. horridus*	170	11.4	12.4	34	67.5	52	55
USNM 2412	*T. horridus*		7.8	12.7	28	58.5	44.5	46
USNM 4928	*T. horridus*		15	14.4	37.5	77.5	50	58
YPM 1821	*T. horridus*			9.5	34		38.5	
DMNH 48617	*T. horridus*		22.28		61.35			51.46
USNM 4720	*T. horridus*		15.68		54.74			
CM 1221	*T. prorsus*		26	13.6		60.5	38.5	48
LACM 7207	*T. prorsus*		31	13		57		51
MOR 004	*T. prorsus*	130	32	7.8	90			45
MOR 1604	*T. prorsus*	152	53.5	7.2	81			48.5
MOR 2923	*T. prorsus*	145	35	7.8	88.5		31	
MOR 2978	*T. prorsus*	131	28.5	7.5	84.5			42
SMM P62/1/1	*T. prorsus*			30.5	8.9		65	42
YPM 1822	*T. prorsus*			26	10.3	24	51.5	36
YPM 1823	*T. prorsus*				8	27	47.5	39
UND 3000	*T. prorsus*			45.27		85.91		

Specimen ID	V8	V9	V10	V11	V12	V13	V14	V15	V16	V17
CMN 34824	51.5	54								
EM P15.1	45	43.5	74.5	12.2		18.5	16	74.5		
CMN 8741					100.4	13.5	10	50	82	35
CMN 56508					136		14			42
RSM P2982.1				8.7	43.5	8.8	5.7	25.9	39	17
RSM P1163.4	50	43.5	66.5	10.5	97	19.5	11	66	90.5	35.5
AMNH 5116		32							91	29
FMNH P12003	42	35							140	34
MOR 1120	33.5	27.5	40	3.9	85	16.5	12	51		
USNM 1201	38	28		14.6					97	31.5
USNM 2100	39	31.2	54	5.5	113	14	13.5	79	84.5	29
USNM 2412	32	31							97	24.5
USNM 4928	34	35							106	27.5
YPM 1821		33							87	26
DMNH 48617	40.47	3.74	52.47	6.757	109.69	14.609	15.028	71.455	97.774	60.22
USNM 4720						19.2	10.7	64.856	96.7	35.7
CM 1221	36	43							99	31.5
LACM 7207	37	45							100	37
MOR 004	35	28.5	50.5	10	116	19	14	45	98	39.5
MOR 1604	28	38	67	9.3	93	18	14	58.5	85.5	59
MOR 2923				9.1	107	16.8	13.7	56		
MOR 2978	40.5	29	42.5	9.3	105.5	19.5	13.6	52	70	45
SMM P62/1/1	49	49	41							97
YPM 1822	36	32	31							72
YPM 1823	33	37	26							77
UND 3000	47.01	34.14	29.43	61.282	8.945					109.39

Specimen ID	V18	V19	V20	V21	V22	V23	V24	V25	V26	V27
CMN 34824										
EM P15.1				90			64			
CMN 8741	26	55			79					
CMN 56508					103					
RSM P2982.1					36					
RSM P1163.4	29.5	67	57	68	102	10.5	46.5	49		
AMNH 5116	18			66					63	70
FMNH P12003	22			64					53.5	84
MOR 1120			58	60	81	5.4	31.5	107.5	45	49
USNM 1201	17			60					58.5	
USNM 2100	19	55	53	64	91	7	94	82	65	88
USNM 2412	21.5			55					48	66.5
USNM 4928	21.5			63.5						71
YPM 1821	20			54						58
DMNH 48617	26.555	63.09	75.05	68.248	85.194					
USNM 4720	29.6	60.6	51.4	6.242	93.102					
CM 1221	21			59					43	57.5
LACM 7207	28			61						
MOR 004	38	61.5	68	76	94		46	49	43	42
MOR 1604	45	89	60	72	78					
MOR 2923							64			
MOR 2978	37.5	58.7	54.8	56	83	9.8	39.4	49.3	47.1	37.5
SMM P62/1/1	21			70					54	80
YPM 1822	17			49						50
YPM 1823	28			49					50.5	61
UND 3000	33.076	56.882	53.059	65.995	94.291					

Specimen ID	V28	V29	V30	V31
CMN 34824	7.6	7.6		20
EM P15.1				
CMN 8741				
CMN 56508				
RSM P2982.1				
RSM P1163.4				
AMNH 5116	9.6	9.6	65	21
FMNH P12003	10.4	10.4	74	29.5
MOR 1120	9	9		
USNM 1201	10.2	10.2	52	22
USNM 2100	10.1	10.1	68	24.5
USNM 2412	10	10	63	27
USNM 4928	9.7	9.7	53	27
YPM 1821	9	9	52	18
DMNH 48617				
USNM 4720				
CM 1221	10.7	10.7	45	29
LACM 7207	9.9	9.9		
MOR 004	10.5	10.7		
MOR 1604				
MOR 2923				
MOR 2978				
SMM P62/1/1	10	10	74	25.5
YPM 1822	8.4	8.4	40	19.5
YPM 1823	8.1	8.1	50	23
UND 3000				

Appendix Table 2.3: first seven principal component scores (accounting for >95% of total variance) of PCA1

Specimen ID	Species	PC 1	PC 2	PC 3	PC 4	PC 5	PC 6	PC 7
CMN 34824	*?*	1.3716	-2.1477	3.2398	2.7834	-0.40684	-0.41763	0.38305
EM P15.1	*?*	2.6332	1.5704	0.076998	1.7971	0.81158	0.45732	0.68143
CMN 8741	*?*	-0.11439	-0.36759	-0.71751	0.38028	-0.44538	-0.03734	-0.49453
CMN 56508	*?*	0.66446	0.51382	0.34761	-0.05862	-0.05437	0.083092	0.10847
RSM P2982.1	*?*	-1.409	-4.2654	-4.4499	1.7212	-0.77195	0.89363	-0.8336
RSM P1163.4	*?*	1.4689	1.0336	-0.16799	2.5344	-0.1332	-0.29592	-0.75803
AMNH 5116	*T. horridus*	-2.3135	-0.35371	-0.10472	-0.02201	0.69543	0.68513	0.36198
FMNH P12003	*T. horridus*	-2.9206	3.1943	0.79169	0.47238	0.20998	-0.47917	-0.80493
MOR 1120	*T. horridus*	0.93773	-2.0008	1.7967	-1.908	0.098117	-0.90306	-2.573
USNM 1201	*T. horridus*	-2.4552	0.82164	0.24481	-0.73937	0.41889	0.029884	-0.79909
USNM 2100	*T. horridus*	-3.3141	1.2922	-0.31866	0.49415	0.39101	0.62606	0.09695
USNM 2412	*T. horridus*	-2.7913	-0.19209	-0.51316	-1.498	0.83672	-0.22024	0.14069
USNM 4928	*T. horridus*	-2.8327	1.5576	0.18853	0.058499	0.65003	-0.25251	0.61342
YPM 1821	*T. horridus*	-1.2852	-1.1092	1.0035	-0.07465	0.38406	-0.33884	-0.50189
DMNH 48617	*T. horridus*	-0.28982	2.3454	1.1746	-1.1426	-2.8184	3.4019	0.08568
USNM 4720	*T. horridus*	-1.6232	0.49677	-0.52708	-0.33754	-3.5419	-3.0291	0.97183
CM 1221	*T. prorsus*	-0.30172	1.3106	-1.0416	-0.50727	1.3512	-0.54558	0.5118
LACM 7207	*T. prorsus*	0.86997	0.8034	-0.40376	0.11039	0.86938	-0.46854	1.1952
MOR 004	*T. prorsus*	2.9563	0.959	-0.89448	-1.2117	0.34088	-0.01761	-0.45336
MOR 1604	*T. prorsus*	3.5889	0.90821	-1.1845	-1.4327	0.023758	-0.04536	0.68812
MOR 2923	*T. prorsus*	2.8614	0.45852	-0.37371	-0.47205	0.3588	-0.31243	-0.3163
MOR 2978	*T. prorsus*	3.1842	-0.54575	-0.42642	-0.2785	-0.68078	0.082005	-0.47678
SMM P62/1/1	*T. prorsus*	-0.21112	1.2073	0.4503	1.7625	0.45325	0.2547	-0.49609
YPM 1822	*T. prorsus*	-0.81516	-4.0694	0.84237	-1.2143	0.91479	0.26991	1.0912
YPM 1823	*T. prorsus*	-0.07567	-4.3934	1.3864	-0.4261	-0.22456	0.62535	1.0761
UND 3000	*T. prorsus*	2.216	0.97236	-0.41982	-0.79105	0.26942	-0.04557	0.50161

Appendix Table 2.4: first six principal component scores (accounting for >95% of total variance) of PCA2

Specimen ID	Species	PC 1	PC 2	PC 3	PC 4	PC 5	PC 6
CMN 34824	*?*	-1.1549	1.4792	0.8372	-0.16464	1.7539	-0.11616
EM P15.1	*?*	1.3117	2.5396	1.8545	0.92832	-0.16314	-0.92775
CMN 8741	*?*	-1.4441	0.12838	0.48961	-0.38883	-0.27956	-0.15742
CMN 56508	*?*	2.3081	0.23998	-0.35394	-0.00785	0.009172	-0.27253
RSM P2982.1	*?*	-11.113	0.15494	1.4507	-0.39841	-0.60974	-0.16675
RSM P1163.4	*?*	1.0187	1.8201	2.1113	0.14178	1.3706	0.22494
AMNH 5116	*T. horridus*	-0.06334	-1.5587	-0.30394	0.59472	-0.0531	-0.6634
FMNH P12003	*T. horridus*	1.669	-2.0843	1.8159	-0.70769	0.50521	1.0331
MOR 1120	*T. horridus*	-0.66288	-1.4979	-2.3299	-3.7105	0.98637	0.86295
USNM 1201	*T. horridus*	0.57856	-1.1774	0.43972	1.5959	0.32723	0.47577
USNM 2100	*T. horridus*	0.72982	-2.8391	0.9178	-0.43082	-0.08121	-1.1945
USNM 2412	*T. horridus*	-0.04591	-3.0462	-0.68822	0.84839	-0.47603	0.11408
USNM 4928	*T. horridus*	0.98489	-2.459	1.3524	0.39059	-1.0305	0.69098
YPM 1821	*T. horridus*	0.13593	-1.7384	-0.00846	-0.00716	0.44282	-0.1435
DMNH 48617	*T. horridus*	2.6038	-0.47255	0.51903	-1.6945	-0.81218	-2.3127
USNM 4720	*T. horridus*	0.90064	-0.92815	0.38379	-0.30577	0.067519	0.65433
CM 1221	*T. prorsus*	0.50394	0.1415	0.24931	1.0125	-0.71823	0.88819
LACM 7207	*T. prorsus*	0.60178	0.78272	0.45043	0.85837	-0.92501	0.59888
MOR 004	*T. prorsus*	0.84081	1.9592	-1.1537	-0.11794	-0.17127	0.80132
MOR 1604	*T. prorsus*	0.35624	2.4507	-1.2125	-0.95118	-2.3287	0.10928
MOR 2923	*T. prorsus*	0.57421	1.7539	-0.35686	-0.52902	-0.32858	0.098972
MOR 2978	*T. prorsus*	0.061349	2.1442	-0.95659	-0.44167	0.63656	-0.51102
SMM P62/1/1	*T. prorsus*	0.61944	1.3876	0.89579	0.029362	1.4164	0.18368
YPM 1822	*T. prorsus*	-1.125	-0.77123	-2.6892	1.9655	0.018147	-0.30835
YPM 1823	*T. prorsus*	-1.2437	0.001887	-3.0701	1.5956	1.2952	-0.66783
UND 3000	*T. prorsus*	1.0541	1.5891	-0.64406	-0.10506	-0.8518	0.70538

Appendix Table 2.5: first six principal component scores (accounting for >95% of total variance) of PCA3

Specimen ID	Species	PC 1	PC 2	PC 3	PC 4	PC 5	PC 6
CMN 34824	*?*	1.7404	0.15425	-0.41844	1.8421	-0.92823	0.30476
EM P15.1	*?*	3.4934	2.4912	0.30718	-0.48815	0.25539	0.25673
CMN 8741	*?*	0.27867	-0.28311	0.02802	0.19694	-0.01213	-0.34408
CMN 56508	*?*	-0.1355	0.11562	-0.08905	0.022569	0.023001	0.037565
RSM P2982.1	*?*	1.3003	-3.1195	1.4883	0.91067	-0.39562	-2.3316
RSM P1163.4	*?*	2.5286	2.3283	-0.60584	0.65374	-0.12397	0.25354
AMNH 5116	*T. horridus*	-1.4348	-0.1599	0.89631	-0.07122	-0.07573	0.004647
FMNH P12003	*T. horridus*	-1.8934	2.0216	-0.15951	1.1757	0.1486	0.056462
MOR 1120	*T. horridus*	-3.0252	-2.5777	-2.9983	0.97766	1.2711	0.17108
USNM 1201	*T. horridus*	-1.1184	0.72986	1.1792	0.28435	-1.4958	1.6509
USNM 2100	*T. horridus*	-2.2426	1.6658	0.35102	-0.00683	0.73965	-0.52242
USNM 2412	*T. horridus*	-2.6703	-0.22586	1.5693	-0.26667	0.29005	0.149
USNM 4928	*T. horridus*	-2.0494	1.8085	1.0018	0.038705	0.90923	-0.43062
YPM 1821	*T. horridus*	-1.6446	0.38642	0.028235	0.32389	0.32582	0.50899
DMNH 48617	*T. horridus*	-1.6863	1.579	-2.1498	-2.8457	-2.0207	-1.3038
USNM 4720	*T. horridus*	-1.3113	0.73263	-0.183	0.11721	0.17128	-0.00684
CM 1221	*T. prorsus*	0.51221	0.30772	1.0737	0.094344	0.28904	-0.50862
LACM 7207	*T. prorsus*	0.98153	0.3077	1.0345	0.10467	0.31925	-0.73989
MOR 004	*T. prorsus*	1.2183	-1.2592	-0.89293	-0.13825	0.057099	-0.05273
MOR 1604	*T. prorsus*	2.248	-0.7365	-0.23877	-1.8968	2.0339	0.75398
MOR 2923	*T. prorsus*	1.5155	-0.37484	-0.81373	-0.1556	0.49704	0.26198
MOR 2978	*T. prorsus*	0.46077	-1.2756	-1.513	0.73418	-0.69924	0.34347
SMM P62/1/1	*T. prorsus*	1.5129	0.67478	-0.75629	1.2858	-0.62159	-0.149
YPM 1822	*T. prorsus*	-0.47427	-2.1739	1.5982	-1.0283	-0.36037	0.76269
YPM 1823	*T. prorsus*	0.19099	-2.7445	0.58127	-0.77557	-1.1932	1.0482
UND 3000	*T. prorsus*	1.7041	-0.37274	-0.31849	-1.0894	0.59605	-0.17428

Appendix Table 2.6: Loading scores of first seven PC within PCA 1

Variable	PC 1	PC 2	PC 3	PC 4	PC 5	PC 6	PC 7
V2	0.38306	0.014594	-0.14931	0.19549	0.024677	0.14648	0.41777
V3	-0.35151	0.16963	-0.06551	0.013605	0.085574	0.006547	0.4682
V4	0.38261	0.21675	-0.00435	0.19174	-0.11461	-0.11549	-0.12318
V5	-0.13711	0.36389	0.30928	0.008951	-0.10168	-0.21896	-0.36412
V6	-0.37437	0.1786	-0.06361	0.15073	-0.1557	0.14852	0.18746
V7	-0.03137	0.36961	-0.19824	0.36808	0.024361	0.069762	0.19877
V8	0.019061	0.083984	0.23538	0.67798	-0.14316	0.10523	-0.19444
V9	0.056441	-0.05536	-0.06379	0.33402	0.54715	-0.63724	0.089484
V14	0.12789	0.22314	0.4547	-0.23607	0.25618	0.12149	0.40745
V16	-0.02744	0.36422	0.3967	-0.17287	0.13303	-0.24391	0.032686
V17	0.2867	0.32703	0.14686	-0.09699	-0.26394	0.10576	0.020241
V18	0.39748	0.086426	-0.10787	-0.00089	-0.26086	-0.08805	0.19399
V21	0.12508	0.07518	0.06247	0.095055	0.60852	0.60567	-0.27211
V27	-0.38311	0.14366	0.018283	0.16786	-0.10175	0.10757	0.060737
V28	-0.00785	0.38152	-0.43115	-0.17624	0.10429	-0.02801	-0.16523
V29	0.007777	0.37983	-0.43298	-0.17898	0.10638	-0.02768	-0.16697

Appendix Table 2.7: Loading scores of first seven PC within PCA 2

Variable	PC 1	PC 2	PC 3	PC 4	PC 5	PC 6
V2	0.000908	0.53904	-0.0159	0.12574	-0.21167	-0.10229
V3	0.058648	-0.35364	0.31018	0.39726	-0.31043	0.048481
V4	0.11148	0.47566	0.18525	-0.27767	-0.0361	0.23593
V5	0.26189	-0.21775	0.30962	-0.28551	0.10385	0.32024
V7	0.14814	0.043617	0.59351	0.032819	-0.33195	-0.12608
V8	0.004416	0.15944	0.46009	0.013765	0.75185	-0.28259
V9	-0.32612	0.082945	0.1981	0.13315	0.015192	0.466
V11	0.000407	0.31401	0.15297	0.62927	-0.0152	0.10273
V12	0.36791	-0.01408	-0.14119	0.17214	0.060046	-0.07831
V13	0.30064	0.19508	-0.23273	0.20016	0.20192	0.31269
V14	0.34885	0.068642	-0.1964	0.13946	-0.05591	-0.18731
V15	0.33273	-0.19174	0.12869	0.082476	0.005442	-0.32497
V16	0.34746	-0.10888	0.059979	-0.08866	-0.01431	0.46514
V17	0.25651	0.29322	0.068831	-0.36644	-0.3064	-0.16743
V22	0.37757	-0.0185	-0.09593	0.12119	0.17085	0.12856

Appendix Table 2.8: Loading scores of first six PC within PCA 3

Variable	PC 1	PC 2	PC 3	PC 4	PC 5	PC 6
V2	0.51641	-0.04888	-0.10122	-0.29312	0.032694	-0.0268
V3	-0.2403	0.31417	0.55017	-0.04217	-0.16663	-0.32557
V4	0.38541	0.14509	-0.47946	0.083418	0.13282	-0.09531
V5	-0.24537	0.46381	-0.30355	0.16132	0.16004	0.21255
V7	0.13217	0.53199	0.10002	-0.04496	0.27249	-0.49209
V8	0.18941	0.3003	-0.19472	0.52518	-0.60728	-0.12389
V9	0.22362	-0.03992	0.36663	0.6585	0.53379	0.23891
V10	0.43655	0.21148	0.19855	-0.31172	0.13686	0.0091
V11	0.37264	0.099713	0.37443	-0.01349	-0.42045	0.43561
V15	-0.18451	0.483	-0.05563	-0.26553	0.066551	0.57844

Appendix Table 2.9: Linear discriminant analysis scores of three independent LDA

Specimen ID	Species	LDA 1	LDA 2	LDA 3
CMN 34824	*?*	5.7736	3.206	5.0528
EM P15.1	*?*	6.4572	3.7086	4.79
CMN 8741	*?*	-0.04719	1.6112	2.7181
CMN 56508	*?*	1.3557	-0.51396	0.57908
RSM P2982.1	*?*	-0.38851	8.0614	12.877
RSM P1163.4	*?*	3.4609	2.4316	3.1007
AMNH 5116	*T. horridus*	-1.0062	-1.1481	-1.2346
FMNH P12003	*T. horridus*	-3.7152	-3.7187	-5.185
MOR 1120	*T. horridus*	-2.577	-2.9314	-3.914
USNM 1201	*T. horridus*	-3.6998	-0.39187	-3.4611
USNM 2100	*T. horridus*	-2.589	-4.1834	-5.0201
USNM 2412	*T. horridus*	-3.1952	-2.9188	-3.8391
USNM 4928	*T. horridus*	-1.6453	-3.0173	-4.6184
YPM 1821	*T. horridus*	-0.90423	-1.8733	-3.609
DMNH 48617	*T. horridus*	-3.1468	-2.91	-4.1815
USNM 4720	*T. horridus*	-3.131	-1.2956	-2.6949
CM 1221	*T. prorsus*	1.0534	1.3384	3.1361
LACM 7207	*T. prorsus*	3.6287	2.0511	4.4641
MOR 004	*T. prorsus*	2.2837	3.0043	4.824
MOR 1604	*T. prorsus*	3.9446	3.6691	3.9551
MOR 2923	*T. prorsus*	3.212	2.5389	3.7101
MOR 2978	*T. prorsus*	3.0187	3.3214	2.9359
SMM P62/1/1	*T. prorsus*	1.5754	2.082	4.0704
YPM 1822	*T. prorsus*	1.5242	1.6081	2.2559
YPM 1823	*T. prorsus*	2.3808	2.3899	3.7972
UND 3000	*T. prorsus*	2.9882	2.3854	4.6089

Appendix Table 2.10: loading scores for all three linear discriminant analyses.

Principal Component	LDA 1	LDA 2	LDA 3
PC1	1.1453	-0.66554	2.1187
PC2	-0.21826	1.3949	-1.2812
PC3	0.088485	-0.05177	0.54995
PC4	0.94914	0.57397	0.44646
PC5	0.73741	-0.10488	-0.35188
PC6	0.003603	0.13637	-1.5617
PC 7	1.2218		

References

Allen, K., & Briggs, D. (1989). *EVOLUTION AND THE FOSSIL RECORD*. Belhaven Press, London.

Alvarez, L., Alvarez, W., Asaro, F., & Michel, H.V. (1980). Extraterrestrial cause for the Cretaceous-Tertiary extinction. *Science* 208:1095–1108.

Arroyave J, Martinez C.M, & Stiassny M.L.J. (2019) DNA barcoding uncovers extensive cryptic diversity in the African long-fin tetra *Bryconalestes longipinnis* (Alestidae: Characiformes). *Journal of Fish Biology* 95:379–392

Ayala, F. (2005). The Structure of Evolutionary Theory. *Theology and Science*. 3(1):104-105. doi:10.1080/14746700500039800.

Bakhtina, Y., Katsnelsonb, M.I., Wolfc, Y.I &. Koonin, E.V. (2020). Evolution in the weak-mutation limit: Stasis periods punctuated by fast transitions between saddle points on the fitness landscape, *The Proceedings of the National Academy of Sciences* 118(4). https://doi.org/10.1073/pnas.2015665118

Barker, M., & Rayens, W. (2003). Partial least squares for discrimination, *Journal of Chemometrics* 17:166-173.

Bennington, J.B., & Bambach, R.K. (1996). Statistical testing for paleocommunity recurrence: Are similar fossil assemblages ever the same? *Palaeogeography, Palaeoclimatology, Palaeoecology* 127(1–4):107-133.

Benton, M. J., Wills, M.A., & Hitchin, R. (2000). Quality of the fossil record through time. *Nature* 403: 534–537.

Brett, C.E., Ivany, L.C., & Schopf, K.M. (1996). Coordinated stasis: An overview. *Palaeogeography, Palaeoclimatology, Palaeoecology* 127(1–4):1–20.

Brown M.B., Arbour, J.H., & Jackson D.A. (2012). Testing of the effect of missing data estimation and distribution in morphometric multivariate data analyses. *Systems in Biology* 61(6):941–954

Brown, C.M., & Vavrek, M.J. (2015). Small sample sizes in the study of ontogenetic allometry; implications for palaeobiology. *PeerJ* 3: e818.

Brusatte, S.L., Richard, B.J., Barrett, P.M., Carrano, M.T., Evans, D.C., Lloyd, G.T., Mannion, P.D., Norell, M.A., Peppe, D.J., Upchurch, P., & Williamson T.E. (2015). The extinction of the dinosaurs. *Biological reviews of the Cambridge Philosophical Society*, 90(2):628-642.

Cantalapiedra, J., Prado, J., Hernández, M., Alberdi, M.. & Cantalapiedra. J. (2017). Decoupled ecomorphological evolution and diversification in Neogene-Quaternary horses. *Science* 355(6325):627–630. https://doi.org/10.1126/science.aag1772

Carsten G., Gasparini, S., Calvet, L., Gurdjos, P., Castan, F., Maujean, B., De Lillo, G., & Lanthony, Y. (2021). AliceVision Meshroom: An open-source 3D reconstruction pipeline. *Proceedings of the 12th ACM Multimedia Systems Conference* Doi:10.1145/3458305.3478443

Chiarenza, A.A., Farnsworth, A., Mannion, P.D., Lunt, D.J., Valdes, P.J., Morgan, J.V., & Allison. P.A. (2020). Asteroid impact, not volcanism, caused the end-Cretaceous dinosaur extinction. *Proceedings of the National Academy of Science.* 117:17084–17093.

Close, R. A., Benson, R.B.J., Saupe, E.E., Clapham, M.E., & Butler. R.J. (2020). The spatial structure of Phanerozoic marine animal diversity. *Science* 368:420–424.

Coiffard, C., Gomez, B., Daviero-Gomez, V., & Dilcher. D.L. (2012). Rise to dominance of angiosperm pioneers in European Cretaceous environments. *Proceedings of the National Academy of Science* 109:20955–20959.

Community, B.O. (2018). Blender - a 3D modelling and rendering package, Stichting Blender Foundation, Amsterdam. Available at: http://www.blender.org.

Condamine, F.L., Guillaume, G., Benton, M.J., & Currie P.J. (2021). Dinosaur biodiversity declined well before the asteroid impact, influenced by ecological and environmental pressures *Nature Communications* 12:3833

Dawson, F., Evans, C., Marsh, R., & Richardson, R. (1994). Chapter 24—Uppermost Cretaceous and Tertiary strata of the Western Canada Sedimentary Basin; in Geological Atlas of the Western Canada Sedimentary Basin, G.D. Mossop and I. Shetsen (comp.), *Canadian Society of Petroleum Geologists and Alberta Research Council, Special Report* 4:387–406., URL http://www.ags.gov.ab.ca/publications/wcsb_atlas/a_ch24/ch_24.html [January 2022].

Dodson, P. (1996) *THE HORNED DINOSAUR*. Princeton University Press. Princeton, New Jersey

Eberth, D.A., & Kamo, S.L. (2019). First high-precision U–Pb CA–ID–TIMS age for the Battle Formation (Upper Cretaceous), Red Deer River valley, Alberta, Canada: implications for ages, correlations, and dinosaur biostratigraphy of the Scollard, Frenchman, and Hell Creek formations. *Canadian Journal of Earth Science* 56:1041–1051.

Eldredge, N., Thompson, J.N., Brakefield, P.M., Gavrilets, S., Jablonski, D., Jackson, J.B.C., Lenski, R.E., Lieberman, B.S., McPeek, M.A., & Miller III., W. (2005). The dynamics of evolutionary stasis. *Paleobiology* 31(2): 133-145.

Emerson, B. C. & Patiño, J. (2018) Anagenesis, Cladogenesis, and Speciation on Islands. *Trends in Ecology and Evolution* 33(7):488–491. doi: 10.1016/j.tree.2018.04.006.

Erwin, D. H., & Anstey, R.L. (1995) *New Approaches to Speciation in the Fossil Record*. New York, Columbia University Press.

Farke, A.A. (2011). Anatomy and taxonomic status of the chasmosaurine ceratopsid *Nedoceratops hatcheri* from the Upper Cretaceous Lance

Formation of Wyoming, U.S.A. *Proceedings of the National Academy of Science* 6:e16196.

Forster, C. (1996a). New information on the skull of *Triceratops*, *Journal of Vertebrate Paleontology*. 16(2):246–258.

Forster, C. (1996b). Species resolution in *Triceratops*: cladistic and morphometric approaches. *Journal of Vertebrate Paleontology*, 16(2):259–270.

Fowler, D.W. (2017). Revised geochronology, correlation, and dinosaur stratigraphic ranges of the Santonian-Maastrichtian (Late Cretaceous) formations of the Western Interior of North America. *Proceedings of the National Academy of Science* 12(11): e0188426. https://doi.org/10.1371/journal.pone.0188426

Futuyma, D. J. (1987). On the role of species in anagenesis. *The American Naturalist*. 130(3):465-473.

Gante, H.F., & Salzburger, W. (2012). Evolution: cichlid models on the runaway to speciation, *Current Biology* 22(22): R956-R958 DOI: https://doi.org/10.1016/j.cub.2012.09.045

Gould, S. J., & Eldredge, N. (1977). Paleontological society punctuated equilibria: The tempo and mode of evolution reconsidered, *Paleobiology* 3(2):115–151.

Grasby, S. E., Them, T.R., Chen, Z., Yin, R., & Ardakani, O.H. (2019). Mercury as a proxy for volcanic emissions in the geologic record. *Earth Science in Review* 196. https://doi.org/10.1016/j.earscirev.2019.102880

Grossnickle, D. M. & Newham, E. (2016). Therian mammals experience an ecomorphological radiation during the Late Cretaceous and selective extinction at the K–Pg boundary. *Proceedings in the Royal Society of Biology* 283(1832) DOI: https://doi.org/10.1098/rspb.2016.0256

Halliday, T.J.D., Upchurch, P., & Goswami, A. (2016). Eutherians experienced elevated evolutionary rates in the immediate aftermath of the Cretaceous–Palaeogene mass extinction. *Proceedings of the Royal Society Biology* 283(1833) DOI: 10.1098/rspb.2015.3026

Hammer, Ø., Harper, D.A.T., & Ryan. P.D. (2001). PAST: paleontological statistics software package for education and data analysis.

Holland, F.D. (1997). A North Dakota *Triceratops* skull. *Rocky Mountain Geology* 32(1):51-60

Horner, J., & Goodwin, M.B. (2006). Major cranial changes during *Triceratops* ontogeny. *Proceedings of the royal society of Biological Science* 273(1602):2757–2761.

Johnson, J. G. (2011). Occurrence of phyletic gradualism and punctuated equilibria through geologic time. *Journal of Paleontology* 56(6):1329–1331.

Langston, W., Jr. (1962). Unpublished "field notes". *Canadian museum of nature archive*.

Lloyd, G., Young, J., & Smith, A. (2012). Taxonomic structure of the fossil record is shaped by sampling bias. *Systematic Biology* 61(1):80–89. https://doi.org/10.1093/sysbio/syr076

Longrich, N.R., & Field, D.J. (2011). *Torosaurus* Is Not *Triceratops*: Ontogeny in chasmosaurine ceratopsids as a case study in dinosaur taxonomy. *Proceedings of the National Academy of Science* 7(2): e32623. doi:10.1371/journal.pone.0032623

Lucas, S.G., Mack, G.H., & Estep, J.W. (1998). The ceratopsian dinosaur *Torosaurus* from the Upper Cretaceous McRae Formation, Sierra County, New Mexico. *New Mexico Geological Society Guidebook, 49th Field Conference*. 223-227,

Mallon, J.C., Holmes, R.B., Bamforth, E.L., & Schumann, D. (2022). The record of *Torosaurus* (Ornithischia: Ceratopsidae) in Canada and its taxonomic implications. *Zoological Journal of the Linnean Society*, 195(1):157–171.

MacFadden, B. (2005). Fossil horses--evidence for evolution. *Science* 307(5716).

Magallón, S., Gómez-Acevedo, S., Sánchez-Reyes, L.L., & Hernández-Hernández. T.A. (2015). metacalibrated time-tree documents the early rise of flowering plant phylogenetic diversity. *New Phytologist* 207:437–453.

Maiorino L., Farke, A.A., Kotsakis, T., & Piras, P. (2013). Is *Torosaurus Triceratops*? geometric morphometric evidence of late maastrichtian ceratopsid dinosaurs. *The Proceedings of the National Academy of Sciences* 8(11): e81608. https://doi.org/10.1371/journal.pone.0081608

Marsh, O. C. (1889). Notice of Gigantic Horned Dinosauria from the Cretaceous, *American Journal of Science*, 36 (224):173-175

Marsh, O.C. (1889). A new family of horned Dinosauria from the Cretaceous. *American Journal of Science*, 3(36):477-478.

Marsh, O.C. (1890). Description of new dinosaurian reptiles. *American Journal of Science*, 3(39):81-86.

Meiri, S., Raia, P., & Santos, A.M.C. (2018). Anagenesis and cladogenesis are useful island biogeography terms. *Trends in Ecology & Evolution* 33(12):895–896. https://doi.org/10.1016/j.tree.2018.09.005

Miller, K.G., Kominz, M.A., Browning, J.V., Wright, J.D., Mountain, G.S., Katz, M.E., Sugarman, P.J., Cramer, B.S., Christie-Blick, N., & Pekar, S.F. (2005). The Phanerozoic record of global sea level change. *Science* 310:1293–1298.

Nadeau, C.P., & Urban, M.C. (2019). Eco-evolution on the edge during climate change. *Ecography* 42(7):1280-1297.

Ostrom, J.H., & Wellnhofer, P. (1986). The Munich specimen of *Triceratops* with a revision of the genus. *Zitteliana* 14:111-158.

Parins-Fukuchi, C., Greiner, E., MacLatchy, L., & Fisher, D. (2019). Phylogeny, ancestors, and anagenesis in the hominin fossil record. *Paleobiology*, 45(2):378-393. doi:10.1017/pab.2019.12

QGIS Development Team. (2020). QGIS Geographic Information System. Open Source Geospatial Foundation Project. http://qgis.osgeo.org

R Core Team. (2019). R: A language and environment for statistical computing. R Foundation for Statistical Computing, Vienna, Austria. URL https://www.R-project.org/.

Rhodes, F.H.T. (1983). Gradualism, punctuated equilibrium and the origin of species. *Nature*. 305(5932):269-272.

Russell, D. A. (1984). The gradual decline of the dinosaurs—fact or fallacy? *Nature* 307:360–361.

Russell, D.A. (1967). A census of dinosaur specimens collected in western Canada. National Museum of Canada, *Natural History Papers* 36:1-13.

Sakamoto, M., Benton, M.J., & Venditti, C. (2016). Dinosaurs in decline tens of millions of years before their final extinction. *Proceedings in the National Academy of Science. USA* 113:5036–5040.

Scannella, J. B., & Horner, J.R. (2010). *Torosaurus* Marsh, 1891, is *Triceratops* Marsh, 1889 (Ceratopsidae: Chasmosaurinae): synonymy through ontogeny, *Journal of Vertebrate Paleontology*, 30(4):1157-1168. DOI: 10.1080/02724634.2010.483632

Scannella, J.B, & Horner, J.R. (2011) '*Nedoceratops'*: An Example of a Transitional Morphology. *Proceedings of the National Academy of Sciences* 6(12): e28705. https://doi.org/10.1371/journal.pone.0028705

Scannella, J. B., Fowler, D.W., Goodwin, M.B., & Horner, J.R. (2014). Evolutionary trends in *Triceratops* from the Hell Creek Formation, Montana, *Proceedings of the National Academy of Sciences of the United States of America* 111(28):10245–10250. doi: 10.1073/pnas.1313334111.

Scannella, J. B., & Fowler, D.W. (2014). A stratigraphic survey of *Triceratops* localities in the Hell Creek Formation, northeastern Montana (2006-2010), *Special Paper of the Geological Society of America*, 503:313–332. doi: 10.1130/2014.2503(12).

Schulte, P., Alegret, L., Arenillas, I., Arz, J.A., Barton, P.J., Bown, P.A., Bralower, T.J., Christeson, G.L., Claeys, P., Cockell, C.S., Collins, G.S., Deutsch, A., Goldin, T.J., Goto, K., Grajales-Nishimura, J.M., Grieve,

R.A.F., Gulick, S.P.S., Johnson, K.R., Kiessling, W., Koeberl, C., Kring, D.A., & MacLeod. K.G. (2010). The Chicxulub asteroid impact and mass extinction at the Cretaceous-Paleogene boundary. *Science* 327:1214–1218.

Schoene, B., Eddy, M.P., Samperton, K.M., Keller, C.B., Keller, G., Adatte, T., & Khadri. S.F.R. (2019). U-Pb constraints on pulsed eruption of the deccan traps across the end-Cretaceous mass extinction. *Science* 363:862–866

Sexton, J.P., McIntyre, P.J. Angert, A., & Rice, K.J. (2009). Evolution and ecology of species range limits. *Annual Review of Ecology Evolution and Systematics*. 40:415-436.

Sheskin, D. (2011). *Handbook of Parametric and Non Parametric Statistical Procedure* (5th ed.). Boca Raton, Florida, CRC Press.

Silvestro, D., Salamin, N., Antonelli, A., & Meyer, X. (2019). Improved estimation of macroevolutionary rates from fossil data using a Bayesian framework. *Paleobiology* 45:546–557

Sloan, R.E., Rigby, J.K., Van Valen, L.M., & Gabriel, D. (1986). Gradual dinosaur extinction and simultaneous ungulate radiation in the Hell Creek Formation. *Science* 232:629–633.

Stacklies, W., Redestig, H., Scholz, M., Walther, D., & Selbig, J. (2007). "pcaMethods – a Bioconductor package providing PCA methods for incomplete data." *Bioinformatics* 23:1164–1167.

Stanley, S. M. (1979). *Macroevolution, pattern and process*. Johns Hopkins University Press. San Francisco

Sternberg, C.M. (1924). Notes on the Lance Formation of southern Saskatchewan. *Canadian Field-Naturalist* 38(4):66-70

Sternberg C.M. (1924). Report on a collection of vertebrates from Wood Mountain, southern Saskatchewan. *Canadian Department of Mines Geological Survey Bulletin (geological Series)* 38(43):27-28.

Sternberg, C.M. (1946). Unpublished field notes. *Canadian museum of nature archive*

Strotz, L.C., & Allen, A.P. (2013). Assessing the role of cladogenesis in macroevolution by integrating fossil and molecular evidence. *Proceedings of the National Academy of Sciences of the United States of America*, 110(8):2904–2909. doi: 10.1073/pnas.1208302110

Sudasinghe, H., Ranasinghe, R.H.T., & Pethiyagoda, R. (2021). Genetic diversity and morphological stasis in the Ceylon Snakehead, *Channa orientalis* (Teleostei: Channidae). *Ichthyological Research* 68:67–80.

Tanke, D.H, & Rothschild, B.M. (2002) *DINOSORES: An Annotated Bibliography of Dinosaur Paleopathology and Related Topics*. New Mexico Museum of Natural History and Science Bulletin 20.

Tokaryk, T.T. (1986). Ceratopsian dinosaurs from the Frenchman Formation (Upper Cretaceous) of Saskatchewan. *Canadian Field-Naturalist* 100(2):192-196.

Valentine, J.W., & Peddicord, R.G. (1967). Evaluation of fossil assemblages by cluster analysis. *Journal of Paleontology* 41(2):502-507.

Wagner, P. (2020). High-resolution dating of Paleozoic fossils. *Evolutionary Biology* 367(6475):249–249.

Wilson, J., & Fowler, D. (2017). First confirmed identification of juvenile *Triceratops* epiparietals. *Cretaceous Research*, 70:71–76. https://doi.org/10.1016/j.cretres.2016.10.005

Xu, X., Forster, C.A., Clark, J.M., & Mo. J. (2006). A basal ceratopsian with transitional features from the Late Jurassic of northwestern China. *Proceedings of the Royal Society B: Biological Sciences*, 273(1598): 2135-2140. doi:10.1098/rspb.2006.3566